NASA TN D-315

TECHNICAL NOTE
D-315

GAS DYNAMICS OF AN INFLATED SPHERE STRIKING A SURFACE

By John T. Howe and E. Dale Martin

Ames Research Center
Moffett Field, Calif.

NATIONAL AERONAUTICS AND SPACE ADMINISTRATION
WASHINGTON
April 1960

NATIONAL AERONAUTICS AND SPACE ADMINISTRATION

TECHNICAL NOTE D-315

GAS DYNAMICS OF AN INFLATED SPHERE STRIKING A SURFACE

By John T. Howe and E. Dale Martin

SUMMARY

A method for predicting the motion of an inflated sphere striking a hard surface has been developed in which the effect of the wave structure in the inflating gas is considered. The method predicts maximum acceleration, the velocity during impact, and the space-time trajectory of the top of the skin. The effects of the presence of an atmosphere are considered. The required size of a sphere that will not exceed a specified allowable acceleration is determined. Results of 52 examples are presented covering a wide range of initial conditions.

INTRODUCTION

The use of an inflated sphere to cushion the impact of equipment being landed on the moon or planets offers a number of advantages derived from the simplicity of such a system. Such a landing vehicle would be compactly packaged aboard a parent vehicle, and inflated with a suitable gas just before the landing is to be made. With a payload supported at its center, the inflated sphere could land unpowered, uncontrolled, and in any attitude. On impact, the sphere would flatten on the bottom, absorbing the impact energy by compressing the gas. When the payload has come to rest, the skin could be ruptured in order to prevent rebound, or the vehicle could be allowed to bounce and roll until it came to rest on level ground.

Furthermore, it is entirely possible that an inflated sphere may serve both as the entry vehicle as well as the impact vehicle for landing on a planet that has an atmosphere. Chapman (ref. 1) in studying entry into planetary atmospheres shows for example that a nonlifting vehicle (such as a sphere) could enter the Martian atmosphere and experience a maximum deceleration only 12 percent of human tolerance. The present analysis concerns itself with the landing impact of an inflated sphere.

Numerous analytical and experimental investigations of the impact behavior of inflated bags and other energy absorbing devices have been made. These are mostly concerned with low-speed impact. Tests have been performed at the University of Texas (refs. 2-9) on various impact absorbing devices at impact speeds up to 130 feet per second.

For high-speed impact, a different analytical approach is useful to reveal features of the impact that become more prominent at higher speed. In the present analysis of the landing impact of an inflated spherical vehicle, several questions need be answered: "What is the motion of the inflated sphere on impact?", "What is the maximum acceleration?", "How much does the sphere deform?", and "What physical parameters are important to an understanding of the behavior of the impacting sphere?" Reference 10 answers these questions for the case of a sphere with a gas of uniform time-dependent pressure and with a skin which remains undeformed away from the impact zone. For high-speed impact, of course, the pressure in the inflating gas is a function of both space and time and cannot be assumed uniform. The present paper is an analysis of the impact motion of an inflated sphere in which the radius of curvature of the top of the sphere is not required to stay constant and wave motion in the inflating gas is taken into account. The questions raised above are answered in an approximate way for high-speed impact conditions.

A wide variety of cases were investigated by numerical integration of the differential equations. The problem was prepared for solution on a digital computer by Mrs. Yvonne Sheaffer.

SYMBOLS

A	top point of the skin
a,b,c,e,f,	points on the trajectory of A in sketch (b)
c	instantaneous local sound speed
$\bar{c}$	$\frac{c}{\lvert u_o \rvert}$, dimensionless local sound speed in the inflating gas
d	point where the shock reflected from the skin strikes the wall in sketch (b)
g	gravitational acceleration
g_e	gravitational acceleration at earth's surface
K	dimensionless parameter in equation (26) defined by equation (27)
l	constant defined by equation (31)
m	mass (without subscript, refers to entire landing system mass)
n	number of g_e's acceleration

p	instantaneous local pressure of the inflating gas
$\bar{p}$	$\frac{p}{p_o}$, dimensionless local pressure
r	radius of curvature of the skin
t	time
$\bar{t}$	$\frac{t\lvert u_o\rvert}{r_o}$, dimensionless time
u	instantaneous local particle velocity (positive in the positive y direction)
$\bar{u}$	$\frac{u}{\lvert u_o\rvert}$, dimensionless local particle velocity
W	shock velocity
$\bar{W}$	$\frac{W}{\lvert u_o\rvert}$, dimensionless shock velocity
y	height of point A above the ground
$\bar{y}$	$\frac{y}{r_o}$, dimensionless height of point A
α	constant defined by equation (31)
β	constant defined by equation (31)
γ	ratio of specific heats of inflating gas
δ	thickness of the skin
ρ	mass density
σ	average tension stress over cross section of skin at point A
ω	constant defined by equation (31)

A 3 4 6

Subscripts

a,d	conditions at those points in sketch (b)
atm	atmospheric conditions
m	material of the skin
min	minimum

p	payload
s	skin (including skin material and payload attached locally)
shock 0,1	shock connecting states 0 and 1
shock 1,2	shock connecting 1 and 2
shock dc at d	conditions at point d of the shock whose trajectory is dc in sketch (b)
0	conditions just before impact
0,1,2,3	states 0,1,2,3 in sketch (b)
6,12,18,24,30, 35,36,41,42	case numbers in figures 20 and 21

ANALYSIS

Statement of the Problem

When the inflated sphere strikes the ground surface, a shock wave passes upward through the inflating gas with velocity W_{01} as shown in sketch (a). Pressure signals from the impact region have not yet been

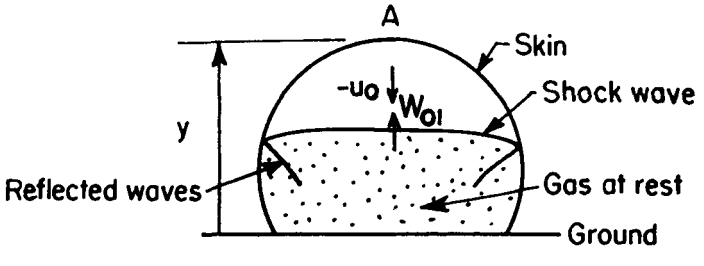

Sketch (a)

received by the gas above the shock wave, so that a portion of the gas continues to fall at undiminished speed. The shock wave is not plane, and there are waves reflected at the boundary. At a high pressure and density, the gas behind the shock is essentially at rest with respect to the ground. Eventually, the shock wave strikes the top surface of the sphere and reflects back toward the ground.

The motion of point A on the skin is to be determined. This motion can be established by making use of a simplified model of the wave shown in sketch (a) as follows:

Along a vertical axis through A, the wave in sketch (a) is assumed to be a plane wave, and reflections from the boundaries are ignored. Then the time-dependent one-dimensional wave motion along the vertical axis through point A would appear as shown in sketch (b).

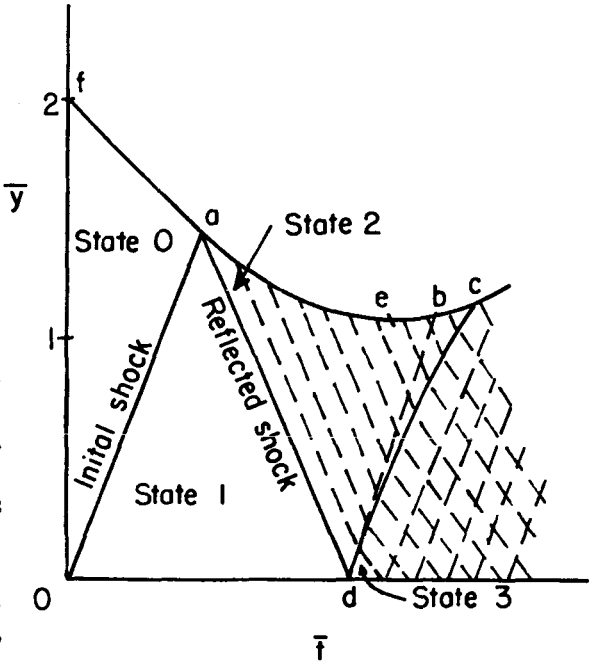

Sketch (b)

At time $t = 0$, the bottom of the sphere makes contact with the horizontal flat surface. The point A on the top of the skin is then at $y = 2r_o$. The path of point A is given by the heavy curve f,a,e,b,c. From f to a, the top of the skin moves at undiminished velocity, $-u_o$, if the acceleration due to the gravity force on the skin and stress waves in the skin are neglected. The line from the origin to a is the trajectory of the initial shock. It is reflected from the skin at a, back to the ground at d, and from the ground at d, back to the skin at c. Along the path a,e,b,c, the skin is accelerating upward with respect to the ground due to an increase in inflating gas pressure over that of state 0. The greatest pressure at the skin is that at a point just to the right of point a below the curve a,e,b,c. Along that curve to the right of point a an observer moving with the skin in the gas would sense a diminishing pressure corresponding to a piston (the skin) being withdrawn from the gas, that is, the piston accelerates in an upward direction. Hence the region a,d,c is a region of rarefaction as indicated by expansion waves shown by the dashed lines. The region to the right of the curve d,c is one in which two families of waves are present. The family of waves traveling downward originated at the skin and was modified on interacting with the shock d,c. The family of waves traveling upward is the reflection of the first family from the ground. As the waves of both families meet, both are modified in strength and speed.

Given the motion of the piston (the skin), one can solve the entire flow field in the y,t plane in sketch (b) by numerical methods. However,

in the present situation the motion of the skin is unknown and is to be determined. Thus it appears that a solution of a differential equation of skin motion that is compatible with the wave equations is needed to yield the desired result.

The Differential Equation of Skin Motion

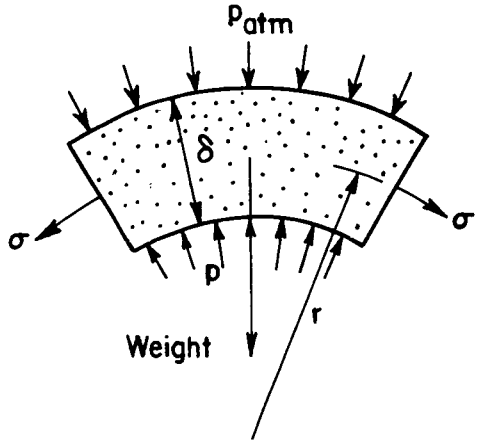

Sketch (c)

The momentum theorem will be applied to a spherical element of skin at the top of the sphere. The stresses on the element are shown in sketch (c). The thickness of the skin, δ, is considered to be small compared with the radius of curvature. It is assumed that the skin can withstand tension only, the average tension stress over the cross section being σ. In general, the gravity force shown is small compared with impact forces during high-speed impact. Within the differential element, ρ_s is assumed to be uniform. A statement of Newton's law is then

$$\frac{d\bar{u}}{d\bar{t}} \equiv \bar{u}\,\frac{d\bar{u}}{d\bar{y}} = \left(\frac{r_o}{\rho_s u_o^2}\right)\left[\frac{p_o(\bar{p} - \bar{p}_{atm})}{\delta} - \frac{2\sigma}{r} - \rho_s g\right] \qquad (1)$$

One may well wonder looking at sketch (c) just where the supported instrument payload fits into the picture. If the payload is distributed over the skin, it is simply included in ρ_s. If, on the other hand, the payload is supported at the sphere center by many inextensible cords from the skin, it is again in effect distributed over the surface of the skin (but not quite uniformly). That portion of the payload mass which is assigned to the point A is then assumed to be included in ρ_s. The distribution function of the center-supported payload mass over the skin surface will not be specified.

Method of Solution

Equation (1) might be solved simultaneously with the unsteady one-dimensional gas dynamic theory on a numerical step basis, provided something is known of the term $-2\sigma/r$. In this way, the entire picture in

the physical plane (sketch (b)) could be constructed. Fortunately, for many useful physical examples, it is not necessary to construct the entire flow field in order to obtain the motion of the skin. Instead, a simplified method is presented and is discussed below.

Reference is again made to sketch (b). States 0 and 1 can be determined directly from shock-wave relationships. From these, the trajectory of the initial shock is determined. Point a is found where this shock trajectory intersects the straight line originating at zero time and having the slope corresponding to the initial velocity of the sphere. Because the skin has a finite mass, and there are no infinite forces acting on it, it undergoes a smooth change in velocity with no discontinuities. Therefore, state 2 just to the right of point a has the same particle (or skin) velocity as a point just to the left of a. That is, $\bar{u}_2 = \bar{u}_0$ where $\bar{u}_2$ is the particle velocity close to a immediately behind the reflected shock ad. This fact and state 1 determine the trajectory of the reflected shock ad, and hence point d is determined readily.

It is worth mentioning that under some circumstances, the first rarefaction to the right of ad may intersect ad for positive values of y/r_o. This would weaken the shock ad causing it to slow down and causing the trajectory to curve slightly to the right. This, it will be seen, would be in favor of the simplified solution in that it delays the time when the shock dc gets back to the skin. However, the trajectory ad is treated as a straight line for all cases.

The initial slope at d of the trajectory of the reflected shock dc is readily found from state 2 and from the fact that the particle velocity of state 3 is zero. This initial slope is represented by the dashed line db. The line db lies to the left of the shock dc because, as the shock meets the rarefactions caused by the upward acceleration of the skin, the shock is weakened and its velocity decreases.

If point c lies to the right of the point of zero skin velocity (point e), the sphere has come to rest before the reflected shock dc gets back to the skin. The foregoing assumptions make the analysis relatively simple. If b lies to the right of e, then c lies to the right of e for reasons given previously. The line db will be checked in each example in order to find where point b lies and, hence, will test the validity of the result; that is, does b, and therefore c, lie to the right of point e?

As long as point c lies at or to the right of point e, the skin motion aec can be solved by the use of simple wave theory without having to construct the entire flow field. This simple wave theory used with the differential equation of skin motion is not affected by events happening below the curve aec as long as these events do not have time to propagate to the skin before it comes to rest. Hence complex wave

interactions in the lower part of the physical plane do not influence the solution of the skin motion. It is necessary to establish the trajectories oa, ad, and db, and to locate points a and d for given values of $\bar{c}_0$ and γ. For this purpose the unsteady one-dimensional shock relations expanded as a series (ref. 11, p. 158) are used. Noting that $\bar{u}_0 = -1$, $\bar{u}_1 = 0$, and $\bar{u}_2 = -1$ leads to

$$\bar{c}_1 = \bar{c}_0 + \frac{\gamma - 1}{2}(\bar{u}_1 - \bar{u}_0) + \cdots = \bar{c}_0 + \frac{\gamma - 1}{2} + \cdots \tag{2}$$

$$\bar{c}_2 = \bar{c}_1 - \frac{\gamma - 1}{2}(\bar{u}_2 - \bar{u}_1) + \cdots = \bar{c}_0 + (\gamma - 1) + \cdots \tag{3}$$

where the minus sign on the second term in equation (3) corresponds to a backward-facing wave. The slope of the shock trajectory connecting states 0 and 1 is

$$\bar{W}_{01} = \left(\frac{d\bar{y}}{d\bar{t}}\right)_{\text{shock } 01} = \frac{\bar{u}_0 + \bar{c}_0 + \bar{u}_1 + \bar{c}_1}{2} = \frac{4\bar{c}_0 + \gamma - 3}{4} \tag{4}$$

The equation of the trajectory Oa is then

$$\bar{y} = \frac{4\bar{c}_0 + \gamma - 3}{4}\bar{t} \tag{5}$$

The trajectory of the top of the skin to point a is given by

$$\bar{y} = 2 - \bar{t} \tag{6}$$

From equations (5) and (6)

$$\bar{y}_a = \frac{2(4\bar{c}_0 + \gamma - 3)}{4\bar{c}_0 + \gamma + 1} \tag{7}$$

and

$$\bar{t}_a = \frac{8}{4\bar{c}_0 + \gamma + 1} \tag{8}$$

The slope of the reflected shock trajectory connecting states 1 and 2 is

$$\bar{W}_{12} = \left(\frac{d\bar{y}}{d\bar{t}}\right)_{\text{shock } 12} = \frac{\bar{u}_1 - \bar{c}_1 + \bar{u}_2 - \bar{c}_2}{2} = -\frac{4\bar{c}_o + 3\gamma - 1}{4} \tag{9}$$

and the trajectory ad is given by

$$\bar{t} = -\frac{4}{4\bar{c}_o + 3\gamma - 1}\bar{y} + \frac{32(2\bar{c}_o + \gamma - 1)}{16\bar{c}_o^2 + 16\bar{c}_o\gamma + 3\gamma^2 + 2\gamma - 1} \tag{10}$$

When $\bar{y} = \bar{y}_d = 0$,

$$\bar{t}_d = \frac{32(2\bar{c}_o + \gamma - 1)}{16\bar{c}_o^2 + 16\bar{c}_o\gamma + 3\gamma^2 + 2\gamma - 1} \tag{11}$$

State 3 at the ground is given by

$$\bar{c}_3 = \bar{c}_2 + \frac{\gamma - 1}{2}(\bar{u}_3 - \bar{u}_2) = \bar{c}_o + \frac{3(\gamma - 1)}{2} \tag{12}$$

The slope at the ground of the reflected shock trajectory dc is

$$\left(\frac{d\bar{y}}{d\bar{t}}\right)_{\text{shock dc at d}} = \frac{\bar{u}_2 + \bar{c}_2 + \bar{u}_3 + \bar{c}_3}{2} = \frac{4\bar{c}_o + 5\gamma - 7}{4} \tag{13}$$

The equation of the straight line db is then

$$\bar{t} = \frac{4}{4\bar{c}_o + 5\gamma - 7}\bar{y} + \frac{32(2\bar{c}_o + \gamma - 1)}{16\bar{c}_o^2 + 16\bar{c}_o\gamma + 3\gamma^2 + 2\gamma - 1} \tag{14}$$

The intersection of this line with the resulting skin trajectory determines the point b, thus supplying the test whether or not b lies to the right of zero skin velocity.

In the region adc, the waves are downward traveling. From simple wave theory (ref. 12, p. 1012)

$$\bar{c} + \frac{\gamma - 1}{2}\bar{u} = \bar{c}_2 + \frac{\gamma - 1}{2}\bar{u}_2 \tag{15}$$

or

$$\frac{\bar{c}}{\bar{c}_2} = \left[1 - \frac{\gamma - 1}{2}\left(\frac{\bar{u} - \bar{u}_2}{\bar{c}_2}\right)\right] \tag{16}$$

but from the isentropic relationships

$$\frac{\bar{p}}{\bar{p}_2} = \left(\frac{\bar{c}}{\bar{c}_2}\right)^{\frac{2\gamma}{\gamma-1}} = \left[1 - \frac{\gamma - 1}{2}\left(\frac{\bar{u} - \bar{u}_2}{\bar{c}_2}\right)\right]^{\frac{2\gamma}{\gamma-1}} \tag{17}$$

Substituting equation (17) into (1) yields

$$\frac{d\bar{u}}{d\bar{y}} = \frac{1}{\bar{u}}\left(\frac{r_o}{\rho_s u_o^2}\right)\left(\frac{p_o}{\delta}\left\{\bar{p}_2\left[1 - \frac{\gamma - 1}{2}\left(\frac{\bar{u} - \bar{u}_2}{\bar{c}_2}\right)\right]^{\frac{2\gamma}{\gamma-1}} - \bar{p}_{atm}\right\} - \frac{2\sigma}{r} - \rho_s g\right) \tag{18}$$

and by definition

$$\frac{d\bar{t}}{d\bar{y}} = \frac{1}{\bar{u}} \tag{19}$$

The boundary conditions are

$$\text{at} \quad \bar{y} = \bar{y}_a, \qquad \bar{u} = \bar{u}_2 = -1 \tag{20}$$

and

$$\text{at} \quad \bar{y} = \bar{y}_a, \qquad \bar{t} = \bar{t}_a \tag{21}$$

It is necessary to know $\bar{p}_2$ in order to integrate equation (18). For the shock connecting states 1 and 0 (ref. 11, p. 158),

$$\left.\begin{aligned} \frac{\bar{p}_1}{\bar{p}_0} &= 1 + \frac{\gamma(\bar{u}_1 - \bar{u}_0)}{\bar{c}_0} + \frac{\gamma(\gamma + 1)}{4}\left(\frac{\bar{u}_1 - \bar{u}_0}{\bar{c}_0}\right)^2 + \cdots \\ \text{or} \\ \frac{\bar{p}_1}{\bar{p}_0} &= \frac{4\bar{c}_0^{\,2} + 4\bar{c}_0\gamma + \gamma^2 + \gamma}{4\bar{c}_0^{\,2}} \end{aligned}\right\} \tag{22}$$

For the shock connecting states 1 and 2

$$\left.\begin{aligned} \frac{\bar{p}_2}{\bar{p}_1} &= 1 - \gamma\left(\frac{\bar{u}_2 - \bar{u}_1}{\bar{c}_1}\right) + \frac{\gamma(\gamma + 1)}{4}\left(\frac{\bar{u}_2 - \bar{u}_1}{\bar{c}_1}\right)^2 - \cdots \\ \text{or} \\ \frac{\bar{p}_2}{\bar{p}_1} &= \frac{4\bar{c}_0^{\,2} + 4(2\gamma - 1)\bar{c}_0 + 4\gamma^2 - 3\gamma + 1}{4\bar{c}_0^{\,2} + 4(\gamma - 1)\bar{c}_0 + (\gamma - 1)^2} \end{aligned}\right\} \tag{23}$$

From equations (22) and (23)

$$\bar{p}_2 = \frac{[4\bar{c}_0^{\,2} + 4(2\gamma-1)\bar{c}_0 + 4\gamma^2 - 3\gamma + 1][4\bar{c}_0^{\,2} + 4\gamma\bar{c}_0 + \gamma(\gamma+1)]}{4\bar{c}_0^{\,2}[4\bar{c}_0^{\,2} + 4(\gamma-1)\bar{c}_0 + (\gamma-1)^2]} \tag{24}$$

Enough information is now assembled to integrate equations (18) and (19) if something is known of the term $2\sigma/r$ in equation (18). In the absence of either theoretical or experimental information about this term, it is assumed to be constant as a first approximation; that is, as the stress at the top of the sphere increases, r also increases and the top of the sphere flattens out. High-speed motion pictures of the impact of a gas-filled elastic ball on a flat surface substantiates that the

top of the ball tends to flatten as the ball decelerates toward rest before rebounding (see sketch (d)). For this reason $2\sigma/r$ is assumed

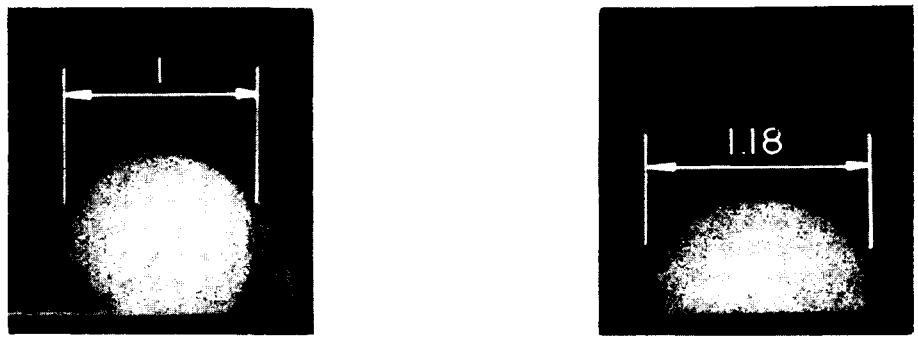

A-26153

Sketch (d).- Impact of playground ball on table (297-gm sphere inflated to atmospheric pressure; impact speed 66.6 ft/sec).

constant for all examples computed in this report. Therefore from simple statics,

$$\frac{2\sigma}{r} = \frac{2\sigma_o}{r_o} = \frac{p_o - p_{atm}}{\delta} = \frac{p_o}{\delta}\left(1 - \bar{p}_{atm}\right) \tag{25}$$

Substituting (25), (3), and $\bar{u}_2 = -1$ into (18) yields

$$\frac{d\bar{u}}{d\bar{y}} = \frac{K}{\bar{u}}\left\{\bar{p}_2\left[1 - \frac{\gamma - 1}{2}\left(\frac{\bar{u} + 1}{\bar{c}_o + \gamma - 1}\right)\right]^{\frac{2\gamma}{\gamma - 1}} - 1 - \frac{\rho_s g \delta}{p_o}\right\} \tag{26}$$

where

$$K = \frac{r_o p_o}{\rho_s \delta u_o^2} = \frac{2}{(1 - \bar{p}_{atm})u_o^2}\left(\frac{\sigma_o}{\rho_s}\right) \tag{27}$$

and $\bar{p}_2$ is given by equation (24). The term $\bar{p}_{atm}$ is treated as a

constant although it will vary slightly with time as a result of motion in the external atmosphere at the skin. Equation (19),

$$\frac{d\bar{t}}{d\bar{y}} = \frac{1}{\bar{u}} \tag{19}$$

is to be integrated simultaneously with equation (26) and the boundary conditions (20) and (21) with the aid of (7) and (8) become

$$\text{at} \quad \bar{y} = \frac{2(4\bar{c}_o + \gamma - 3)}{4\bar{c}_o + \gamma + 1}, \qquad \bar{u} = -1 \tag{28}$$

and

$$\bar{t} = \frac{8}{4\bar{c}_o + \gamma + 1} \tag{29}$$

Variables can be separated in equation (26) and the result can be integrated if the term raised to the power $2\gamma/(\gamma-1)$ is expanded in a series. The result is an approximate expression of $\bar{y}$ as a function of $\bar{u}$. Keeping three terms of the series in the integration yields (if $4\alpha\omega > \beta^2$)

$$\bar{y} = \bar{y}_a + \frac{1}{2\omega} \ln\left(\frac{\alpha+\beta\bar{u}+\omega\bar{u}^2}{\alpha-\beta+\omega}\right) + \frac{\beta}{\omega\sqrt{4\alpha\omega-\beta^2}}\left(\tan^{-1}\frac{\beta-2\omega}{\sqrt{4\alpha\omega-\beta^2}} - \tan^{-1}\frac{2\omega\bar{u}+\beta}{\sqrt{4\alpha\omega-\beta^2}}\right) \tag{30a}$$

or if $4\alpha\omega < \beta^2$

$$\bar{y} = \bar{y}_a + \frac{1}{2\omega} \ln\left(\frac{\alpha+\beta\bar{u}+\omega\bar{u}^2}{\alpha-\beta+\omega}\right) - \frac{\beta}{2\omega\sqrt{\beta^2-4\alpha\omega^2}} \ln\left[\frac{(2\omega\bar{u}+\beta-\sqrt{\beta^2-4\alpha\omega})(\beta-2\omega+\sqrt{\beta^2-4\alpha\omega})}{(2\omega\bar{u}+\beta+\sqrt{\beta^2-4\alpha\omega})(\beta-2\omega-\sqrt{\beta^2-4\alpha\omega})}\right] \tag{30b}$$

where

$$\left.\begin{aligned} \alpha &= K\left\{\bar{p}_2\left[1 + \frac{\gamma^2 + \gamma(1 - 4l)}{4l^2}\right] - \frac{\rho_s g \delta}{p_o} - 1\right\} \\ \beta &= K\bar{p}_2\left[\frac{\gamma^2 + \gamma(1 - 2l)}{2l^2}\right] \\ \omega &= K\bar{p}_2\left(\frac{\gamma^2 + \gamma}{4l^2}\right) \\ l &= \bar{c}_o + \gamma - 1 \end{aligned}\right\} \qquad (31)$$

A 3 4 6

and $\bar{y}_a$ is given by equation (7). Setting $\bar{u}$ equal to zero in equation (30) yields an approximate expression for $\bar{y}_{min}$.

For the case where ρ_s is uniform (payload uniformly distributed over the skin) and the mass of the inflating gas is small compared with the entire mass of the landing vehicle, the parameter K defined by equation (27) has a special meaning. It is simply $(3/2)(\gamma-1)$ times the ratio of the internal energy in the gas before impact to the total kinetic energy of the system before impact. That ratio is the important physical parameter ξ used in reference 10. Hence, K and ξ are simply related by the factor $(3/2)(\gamma-1)$ for the conditions cited above.

Under the same conditions, the ratio of the mass of payload to the mass of the entire vehicle is directly related to K by definition (eq.(27)); that is,

$$\frac{m_p}{m} = 1 - \frac{K u_o^2 (1 - \bar{p}_{atm})}{2(\sigma_o/\rho_m)} \qquad (32)$$

where

$$m = m_s = m_m + m_p \qquad (33)$$

or dividing equation (33) by the surface area of the skin

$$\rho_s = \rho_m + \rho_p \qquad (34)$$

THE SOLUTIONS AND RESULTS

The differential equations (26) and (19) show that exclusive of the gravity term, the physical parameters governing the impact motion are γ, $\bar{c}_o$, and K, given by equation (27). For the examples of interest, the gravity term is very small compared with unity and was neglected in the numerical work, except for one case to be discussed later.

Equations (26) and (19) were integrated numerically using the boundary conditions (28) and (29) for 52 examples having given values of K, $\bar{c}_o$, and γ. The integration was performed on an IBM type 704 electronic data-processing machine using the Adams-Moulton predictor-corrector method of integration.

The values of K, $\bar{c}_o$, and γ for each example are shown in table I. Corresponding possible physical situations of velocity, temperature, atmospheric pressure, material, and initial stress parameters are also shown in the table. It should be pointed out that γ, K, and $\bar{c}_o$ completely specify a problem but that a given K and $\bar{c}_o$ can correspond to any number of real physical situations, and these physical situations listed are simply designed to cover an orderly range of problems.

From the differential equation of motion, (26), it is seen that the maximum acceleration $u_o^2\bar{u}\, d\bar{u}/r_o d\bar{y}$ along aebc occurs where $\bar{u}$ is -1, which is state 2 just to the right of point a. This is expected because the pressure pushing the skin upward is higher there than anywhere else in the region. If the maximum allowable acceleration is ng_e, then

$$\frac{r_o n g_e}{u_o^2} = \left(\bar{u}\,\frac{d\bar{u}}{d\bar{y}}\right)_{\text{state 2}} \tag{35}$$

Also, from equations (26) and (35) for $\bar{u} = -1$, neglecting the gravity term,

$$r_o = \frac{u_o^2 K}{n g_e}(\bar{p}_2 - 1) = \frac{2}{n g_e(1 - \bar{p}_{atm})}\left(\frac{\sigma_o}{\rho_s}\right)(\bar{p}_2 - 1) \tag{36}$$

where $\bar{p}_2$ is given in equation (24) as a function of $\bar{c}_o$ and γ. Equation (36) gives the initial radius required such that the top point of the skin of an impacting sphere will not exceed the allowable acceleration. Figure 1 is a graph of the dimensionless initial radius required (or dimensionless maximum acceleration of eq. (35)) as a function of $\bar{c}_o$ for the different values of K used in the numerical solutions. The

physical data from case 42 (table I) and figure 1 can be used to show that a sphere 10 feet in diameter is needed to absorb an impact velocity of 1000 feet per second if the maximum allowable acceleration is 10,000 earth g's.

The position of the top of the sphere is plotted as a function of the acceleration in figures 2 through 8. It is seen that the acceleration diminishes smoothly from its high value when the initial shock strikes the top of the sphere to its low value as the sphere reaches its maximum deformation just before rebound.

The height of the top of the sphere above the ground during impact as a function of velocity is shown in figures 9 through 15. Each figure corresponds physically to a given impact velocity, u_o, and each curve corresponds to a different initial temperature T_o. As would be expected, the curves become steeper for increasing T_o and increasing u_o. The top two curves in figures 14 and 15 cross because of the nonlinearity of the differential equation (26).

A 3 4 6

The trajectories of the top point of the skin in the $\bar{y},\bar{t}$ plane are shown in figures 16 through 21. Physically, each figure presents curves for a given T_o, and each curve corresponds to a different u_o. The smallest minimum value of $\bar{y}$ for any example is 0.88 in case 37. It appears in figure 16. This is not surprising because case 37 had the smallest value of $\bar{c}_o = c_o/|u_o|$ and the corresponding initial shock velocity is the smallest, as shown by equation (11). For this case, the top of the skin had traveled more than halfway to the ground before the initial shock struck it.

In every case in figures 16 through 21 where point b of sketch (b) fell to the left of the point of zero velocity, it is marked as "b" with a subscript corresponding to the case number. This occurred in 9 out of the 52 examples. These were cases of a high initial gas temperature and hence a high wave speed. The curve to the right of each of these points is in question in that the reflected shock dc may have struck the skin before it came to rest, thus invalidating the theory. However, it appears that in most of the cases where b appears, the skin has come nearly to rest by the time point b is reached and is even nearer to rest before the shock dc arrives. Therefore, the appearance of point b in the examples computed is not considered to invalidate the results.

Figure 22 shows the maximum deformation corresponding to the minimum value of $\bar{y}$ when the skin comes to rest. It is seen that the minimum $\bar{y}$ increases with increasing K and $\bar{c}_o$ in the range of initial conditions used. When the variables in equation (26) are separated and the term pertaining to $\bar{y}$ is integrated, it becomes evident that the minimum $\bar{y}$ diminishes linearly with $1/K$ for a given γ and $\bar{c}_o$; that is,

$$\bar{y}_{min} = \bar{y}_a - \frac{1}{K}\int_0^{-1} \frac{\bar{u}\, d\bar{u}}{\bar{p}_2\left[1 - \left(\frac{\gamma-1}{2}\right)\left(\frac{\bar{u}-1}{\bar{c}_o+\gamma-1}\right)\right]^{\frac{2\gamma}{\gamma-1}} - 1} \qquad (37)$$

where $\bar{y}_a$ given by equation (28) and $\bar{p}_2$ given by equation (24) are both functions of γ and $\bar{c}_o$. Application of formula (37) to any point on a curve in figure 22 immediately yields a value of the definite integral for the corresponding $\bar{c}_o$. Then $\bar{y}_{min}$ for that $\bar{c}_o$ and γ and any K can quickly be determined. Simply setting K equal to infinity in equation (37) yields the envelope of the curves shown by the dashed line in figure 22. The lower values of $\bar{y}_{min}$ for each curve (except K = 2) were determined by use of equation (37).

Comparison of Several Gases

All of the examples discussed so far are for $\gamma = 1.41$, and could apply to either hydrogen or air as the inflating gas. In order to study the effect of using different gases for a given impact condition, examples 43 through 49 were computed. They correspond to a given condition of impact velocity, gas temperature, and pressure (or skin stress parameter). Thus K is the same for all cases, but both γ and $\bar{c}_o$ are different because of the different gases. The gases were chosen to cover a broad range of γ and molecular weights. They are helium, air, argon, carbon dioxide, octane (C_8H_{18}), Freon 12, and dodecane ($C_{12}H_{26}$) in order of ascending molecular weights.

The results for an impact speed of 750 feet per second, initial temperature of 500° R, and skin stress parameter $\sigma_o/\rho_s = 10^6$ ft^2/sec^2 are shown in figures 23 through 25.

The results for the last three gases mentioned indicate that the top of the sphere almost strikes the ground before the initial shock even hits the top. In this situation the applicability of the physical model used in the analysis is doubtful. But if the results are considered to be qualitatively indicative of the behavior, it is seen in figure 23 that a sphere inflated with a very heavy gas experiences a large acceleration. Figures 23 through 25 indicate that a helium-filled sphere behaves much like a hydrogen-filled sphere, and an argon-filled sphere behaves much like an air-filled sphere. The three figures show that a sphere has a much smaller $\bar{y}_{min}$ when inflated with a very heavy gas than when inflated with a light gas.

The effect of changing γ alone for a given $\bar{c}_o$ and K was investigated by computing a series of examples. These will not be presented

graphically. The results indicate that an increase in γ increases the maximum acceleration and $\bar{y}_{min}$ both nonlinearly, but appears to affect the acceleration more than it affects $\bar{y}_{min}$.

Comparison With the Approximation of Uniform Compression

One of the assumptions in reference 10 is that the inflating gas has uniform properties at any instant, varying with time such that $pV^{\gamma} = \text{constant}$. Table II is a comparison between the one-dimensional results of the present analysis with the results of a one-dimensional analysis in which a uniform compression is assumed throughout the gas. In the latter, the differential equation replacing equation (26) is

$$\frac{d\bar{u}}{d\bar{y}} = \frac{K}{\bar{u}}\left[\left(\frac{2}{\bar{y}}\right)^{\gamma} - 1\right] \tag{38}$$

This equation was integrated using the boundary condition

$$\text{at } \bar{y} = 2, \quad \bar{u} = -1 \tag{39}$$

The comparison shows that for a given K (i.e., a given impact velocity), the assumption of uniform compression is very good for high wave speed ($\bar{c}_o$). In particular, for $K = 200$ and $\bar{c}_o = 41.7$, the maximum accelerations differ by only 8 percent, and the values of $\bar{y}_{min}$ are identical. For low wave speeds, the maximum accelerations shown differ by as much as a factor of 5.7, and the values of $\bar{y}_{min}$ by a factor of 1.47. The maximum acceleration of the wave analysis occurs when the initial shock wave strikes the top of the skin. Conversely in the uniform compression analysis the maximum acceleration occurs at the end of the impact as the sphere comes to rest.

CONCLUDING REMARKS

A method has been developed for predicting the motion of the top of an inflated spherical membrane during impact of the bottom with the ground. A differential equation of skin motion is combined with the simple wave theory of unsteady one-dimensional gas dynamics. As a first approximation, the term involving the ratio of skin stress to radius of curvature of the top of the skin is assumed to be constant. When a better understanding of this term is achieved either by theory or experiment, the method can easily be modified accordingly.

Three parameters are found to govern the motion of the sphere on impact. These are γ, $\bar{c}_o$, and K which are the ratio of specific heats of the gas used to inflate the sphere, the ratio of sound speed in the gas before impact to the impact velocity, and a combination of physical properties of the landing system, respectively.

Maximum acceleration, velocity, and space-time relationships resulting from the analysis are presented for 52 cases. The results indicate that for a given impact velocity and allowable acceleration, the size of the sphere required increases at an increasing rate with diminishing $\bar{c}_o$ for a given K and γ, and increases linearly with increasing K for a given $\bar{c}_o$ and γ. As the top of the sphere comes to rest, the minimum distance between it and the ground increases nonlinearly with both K and $\bar{c}_o$ in the range of input conditions used in the examples.

The effect of increasing γ for a given $\bar{c}_o$ and K is to increase the maximum acceleration and minimum distance between the top of the sphere and the ground (both nonlinearly), affecting the maximum acceleration more than the minimum distance. For a given impact velocity, a sphere inflated with a very heavy gas experiences higher acceleration and greater deformation during impact than does a similar sphere inflated to the same pressure and temperature with a light gas.

The results of the analysis were compared with those resulting from the assumption of uniform compression, varying only with time by the isentropic relation. That assumption had been used in reference 10 and the results show that the assumption is very good for high wave speed (large $\bar{c}_o$).

Ames Research Center
National Aeronautics and Space Administration
Moffett Field, Calif., Jan. 13, 1960

REFERENCES

1. Chapman, Dean R.: An Approximate Analytical Method for Studying Entry Into Planetary Atmospheres. NACA TN 4276, 1958.

2. Matlock, Hudson, Ripperger, E. A., Turnbow, James W., and Thompson, J. Neils: High-Velocity Impact Cushioning, Part I. Drop Test Facilities and Instrumentation. Structural Mechanics Res. Lab., Univ. of Texas, 1957.

3. Matlock, Hudson, Ripperger, E. A., Turnbow, James W., and Thompson, J. Neils: High-Velocity Impact Cushioning, Part II. Energy Absorbing Materials and Systems. Structural Mechanics Res. Lab., Univ. of Texas, 1957.

4. Matlock, Hudson, and Thompson, J. Neils: High-Velocity Impact Cushioning, Part III. Preliminary Tests on a Nonpressurized Air Bag. Structural Mechanics Res. Lab., Univ. of Texas, 1957.

5. Karnes, Charles H., Turnbow, James W., Ripperger, E. A., and Thompson, J. Neils: High-Velocity Impact Cushioning, Part V. Energy Absorption Characteristics of Paper Honeycomb. Structural Mechanics Res. Lab., Univ. of Texas, 1959.

6. Morgan, Carl W., and Moore, Walter L.: Cushioning for Air Drop, Part V. Theoretical and Experimental Investigations of Fluid Filled Metal Cylinders for Use as Energy Absorbers on Impact. Structural Mechanics Res. Lab., Univ. of Texas, 1956.

7. Ali, Ahmin, and Matlock, Hudson: Cushioning for Air Drop, Part VI. Preliminary Investigation of the Absorption of Shock Energy by Wood in Lateral Compression. Structural Mechanics Res. Lab., Univ. of Texas, 1957.

8. Turnbow, James W.: Cushioning for Air Drop, Part VII. Characteristics of Foamed Plastics Under Dynamic Loading. Structural Mechanics Res. Lab., Univ. of Texas, 1957.

9. Turnbow, James W., Matlock, Hudson, and Thompson, J. Neils: Cushioning for Air Drop, Part III. Characteristics of Paper Honeycomb Under Dynamic Loading. Structural Mechanics Res. Lab., Univ. of Texas, 1956.

10. Martin, E. Dale, and Howe, John T.: An Analysis of the Impact Motion of an Inflated Sphere Landing Vehicle. NASA TN D-314, 1960.

11. Courant, R., and Friedrichs, K. O.: Supersonic Flow and Shock Waves. Interscience Pub. Inc., N.Y., 1956.

12. Shapiro, Ascher H.: The Dynamics and Thermodynamics of Compressible Fluid Flow. Vol. 2, The Ronald Press Co., N.Y., 1954.

TABLE I.- EXAMPLES OF ANALYSIS

Case number	Quantities necessary to the solution			Possible corresponding physical situation; $p_{atm} = 0$; $\sigma_o/\rho_s = 10^6$ ft^2/sec^2 (1)	
	γ	K	$\bar{c}_o$	T_o, °R	$\lvert u_o \rvert$, ft/sec
1	1.41	200	13.1851376	50	100
2			18.6466005	100	
3			26.370275	200	
4			32.296859	300	
5			37.293201	400	
6			41.695066	500	
7	1.41	50	6.592569	50	200
8			9.3233002	100	
9			13.1851376	200	
10			16.148429	300	
11			18.6466005	400	
12			20.847533	500	
13	1.41	22.222222	4.3950459	50	300
14			6.2155335	100	
15			8.7900917	200	
16			10.7656198	300	
17			12.431067	400	
18			13.898355	500	
19	1.41	12.5	3.296284	50	400
20			4.66165	100	
21			6.592569	200	
22			8.074215	300	
23			9.3233002	400	
24			10.4237666	500	
25	1.41	8	2.6370275	50	500
26			3.7293201	100	
27			5.274055	200	
28			6.4593719	300	
29			7.45864	400	
30			8.3390132	500	

[1]See footnote at end of table, p. 23.

TABLE I.- EXAMPLES OF ANALYSIS - Concluded

Case number	Quantities necessary to the solution			Possible corresponding physical situation; $p_{atm} = 0$; $\sigma_o/\rho_s = 10^6$ ft^2/sec^2 (1)	
	γ	K	$\bar{c}_o$	T_o, °R	$\lvert u_o \rvert$, ft/sec
31	1.41	3.555556	1.758018	50	750
32			2.486213	100	
33			3.516038	200	
34			4.306248	300	
35			4.972427	400	
36			5.559342	500	
37	1.41	2.0	1.318514	50	1000
38			1.864660	100	
39			2.637028	200	
40			3.229686	300	
41			3.729320	400	
42			4.169507	500	
43	1.67	3.555556	4.295070	500	750
44	1.29		1.137880		
45	1.40		1.460750		
46	1.12		.639520		
47	1.03		.516970		
48	1.04		.634560		
49	1.67		1.358220		
50	1.67	200	32.296859		
51		50	6.592569		
52		3.555556	4.306248		

[1]Hydrogen was the inflating gas with the following exceptions:

Case	Gas
43	Helium
44	CO_2
45	Air
46	Freon 12
47	Dodecane
48	Octane
49	Argon

TABLE II.- COMPARISON OF WAVE ANALYSIS WITH UNIFORM COMPRESSION ASSUMPTION FOR THE CASE OF CONSTANT σ/r

[γ = 1.41, hydrogen gas]

K	$\bar{c}_o$ (wave analysis only)	Maximum acceleration $(\bar{u}\, d\bar{u}/d\bar{y})_{max}$		Maximum acceleration ratio ②/①	$\bar{y}_{min}$		$\bar{y}_{min}$ ratio ④/③
		Wave analysis ①	Uniform compression ②		Wave analysis ③	Uniform compression ④	
High wave speed							
200	41.70	13.92	12.86	0.924	1.91	1.91	1.0
50	20.85	7.16	6.35	.886	1.82	1.84	1.01
2	4.17	1.79	1.71	.956	1.22	1.29	1.06
Low wave speed							
200	13.19	46.83	12.86	.275	1.84	1.91	1.04
50	6.59	25.60	6.35	.248	1.70	1.84	1.08
2	1.32	9.72	1.71	.176	.88	1.29	1.47

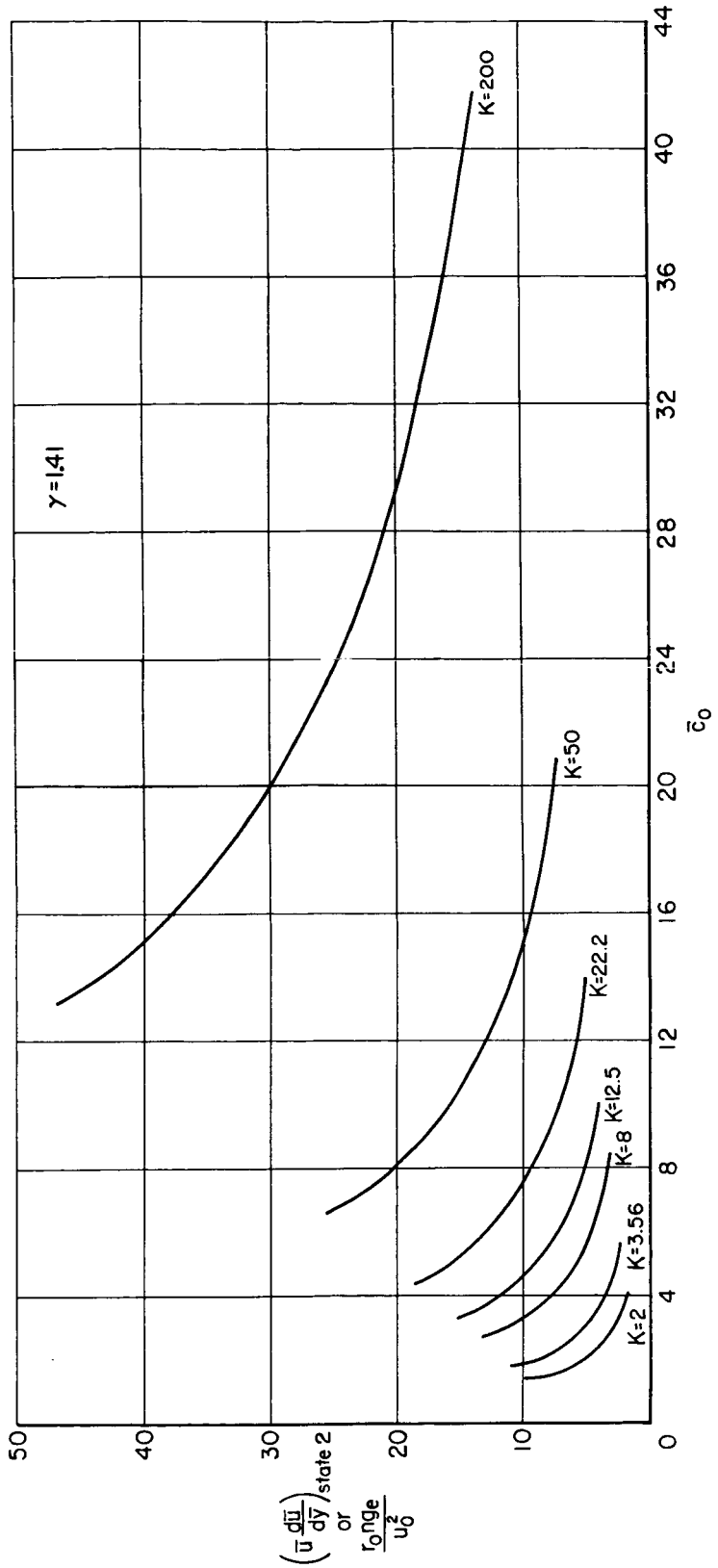

Figure 1.- Maximum acceleration and initial radius required.

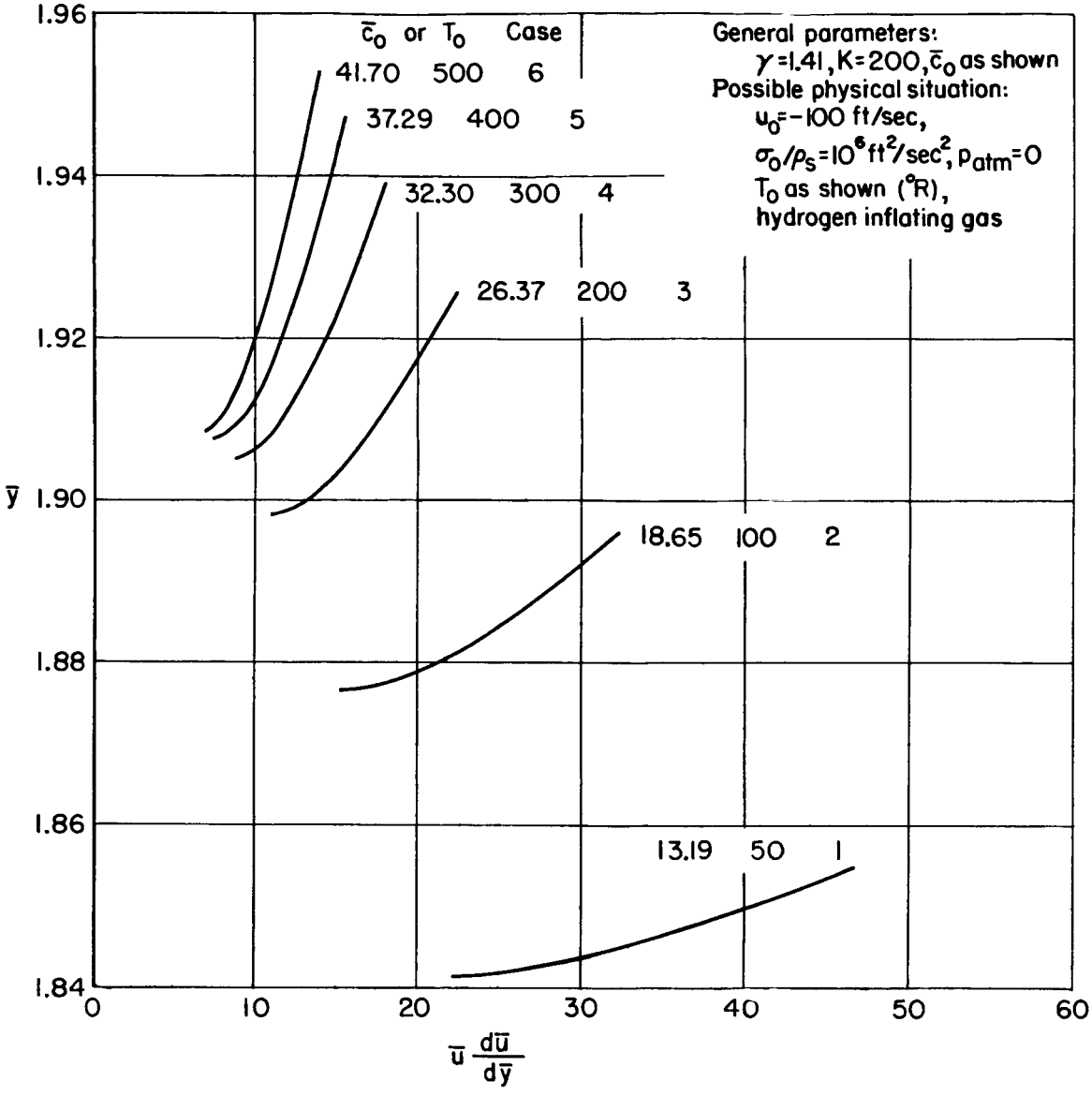

Figure 2.- Acceleration of top of sphere; K = 200.

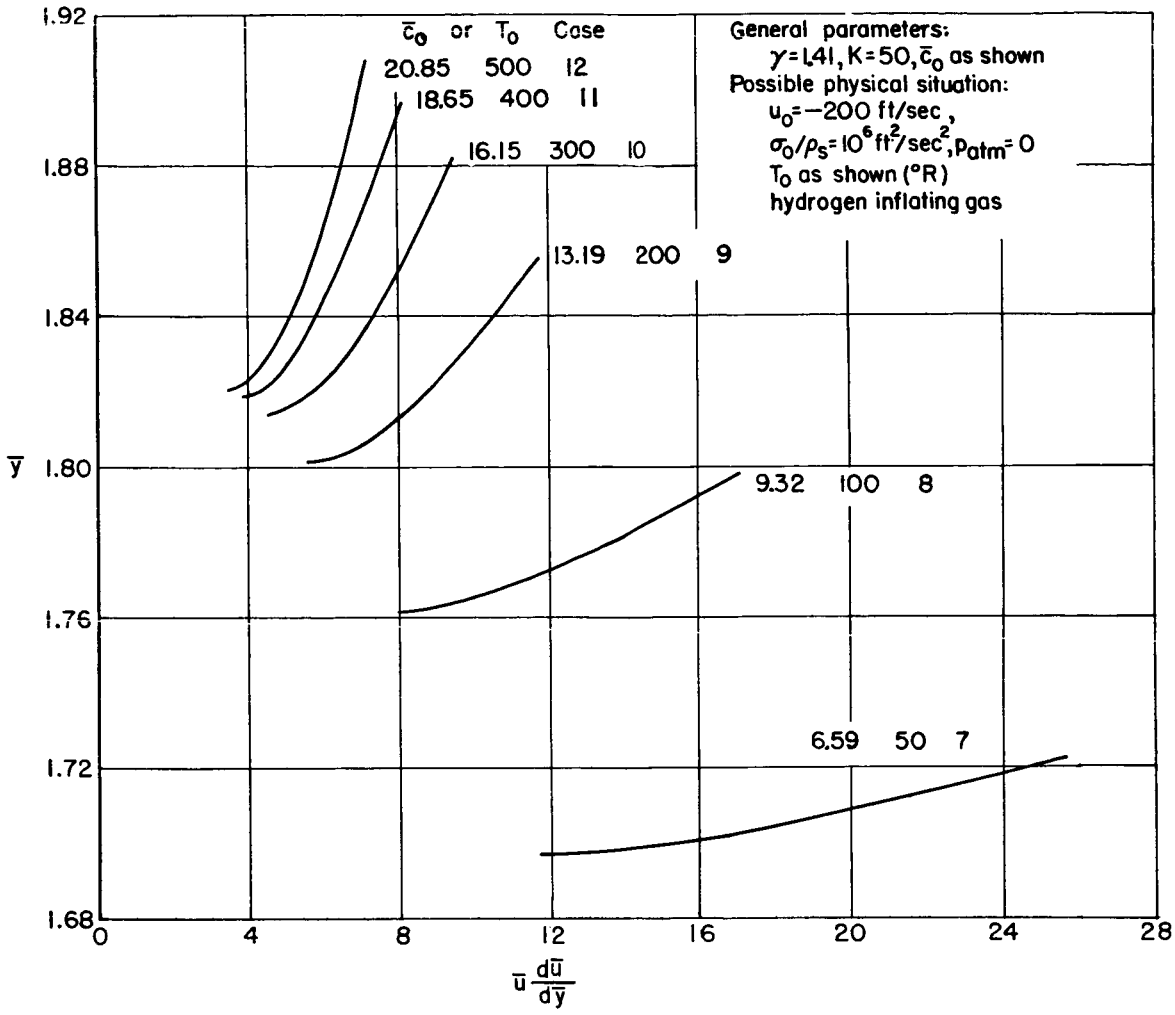

Figure 3.- Acceleration of top of sphere; K = 50.

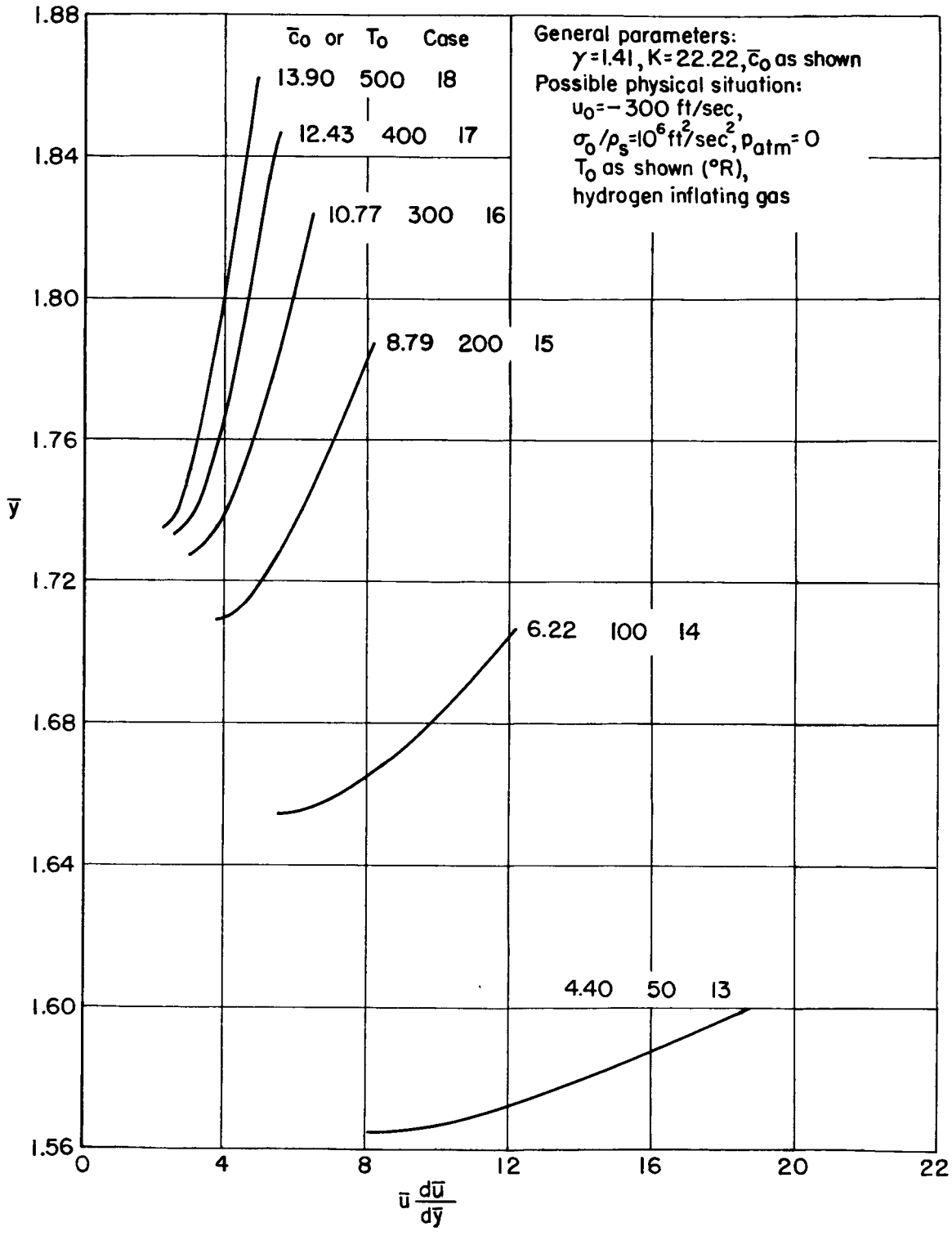

Figure 4.- Acceleration of top of sphere; K = 22.22.

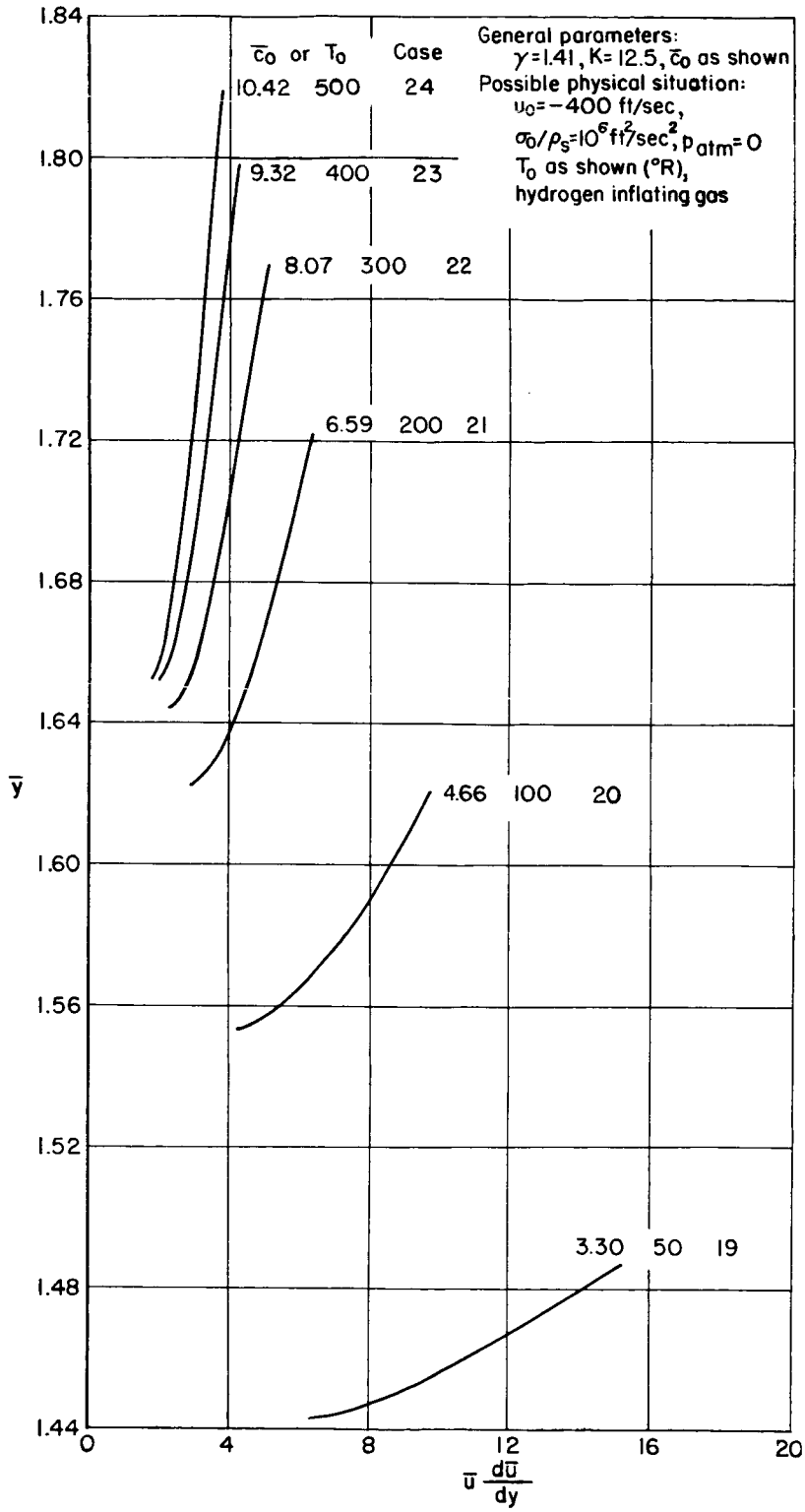

Figure 5.- Acceleration of top of sphere; K = 12.5.

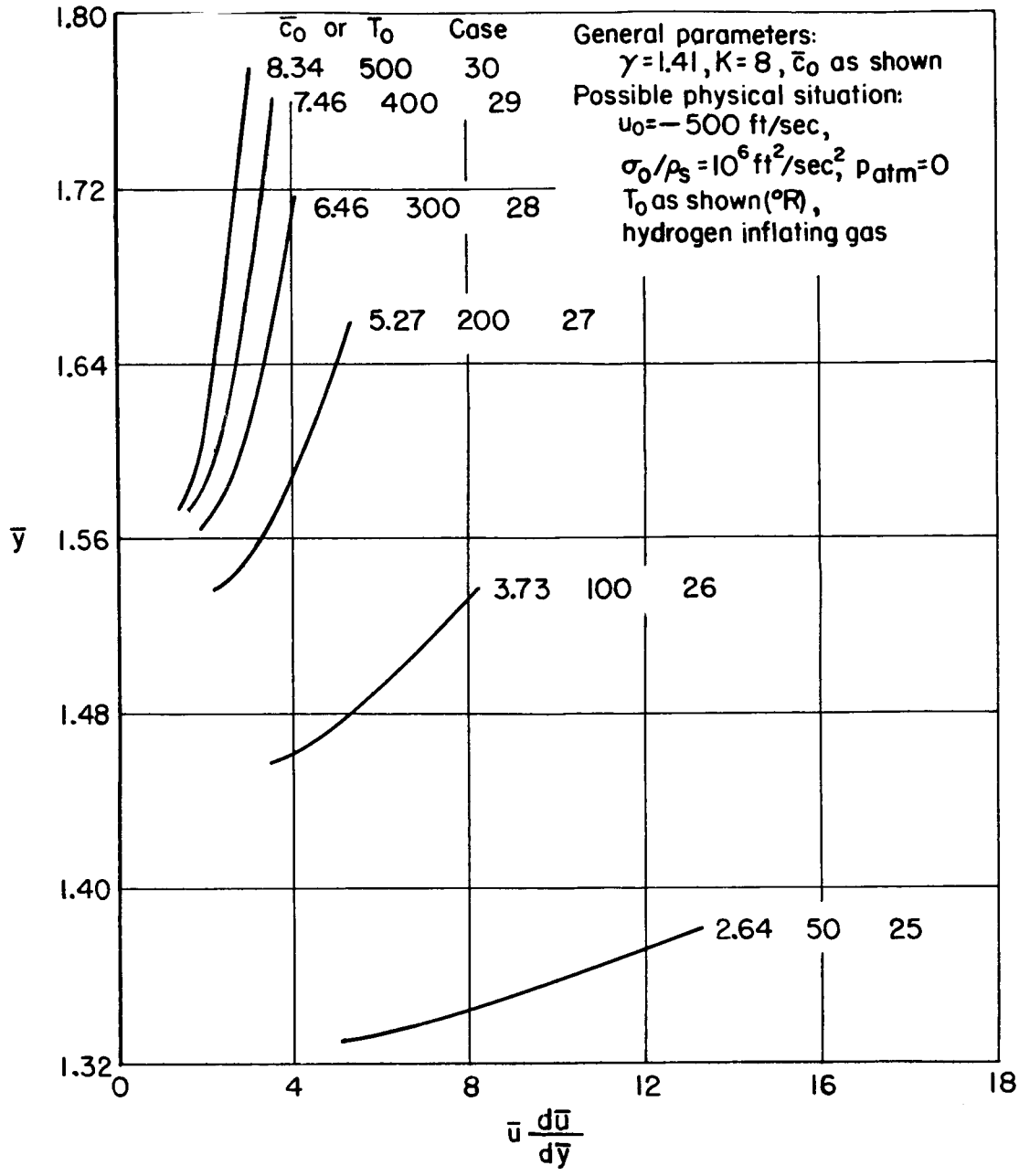

Figure 6.- Acceleration of top of sphere; K = 8.

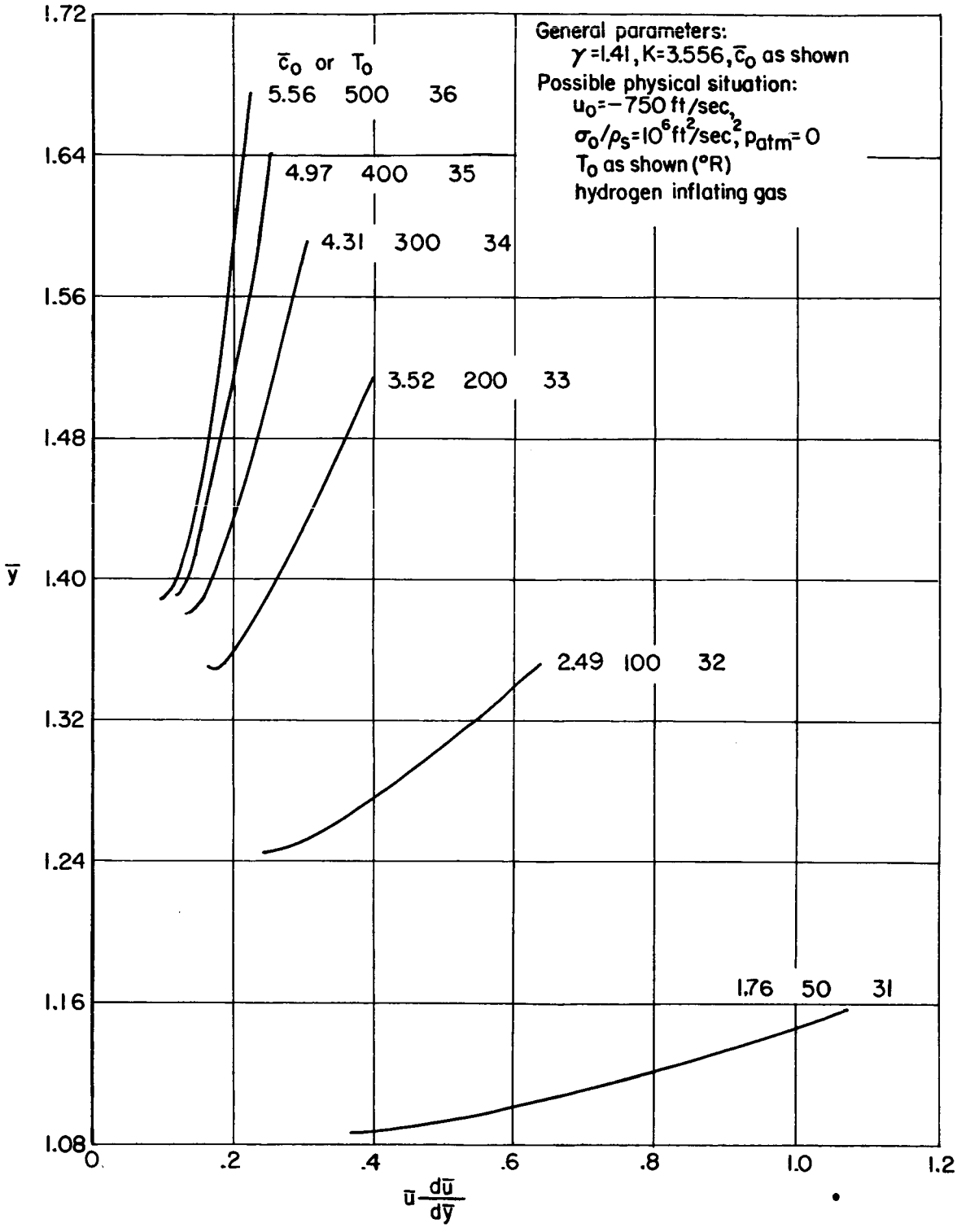

Figure 7.- Acceleration of top of sphere; K = 3.556.

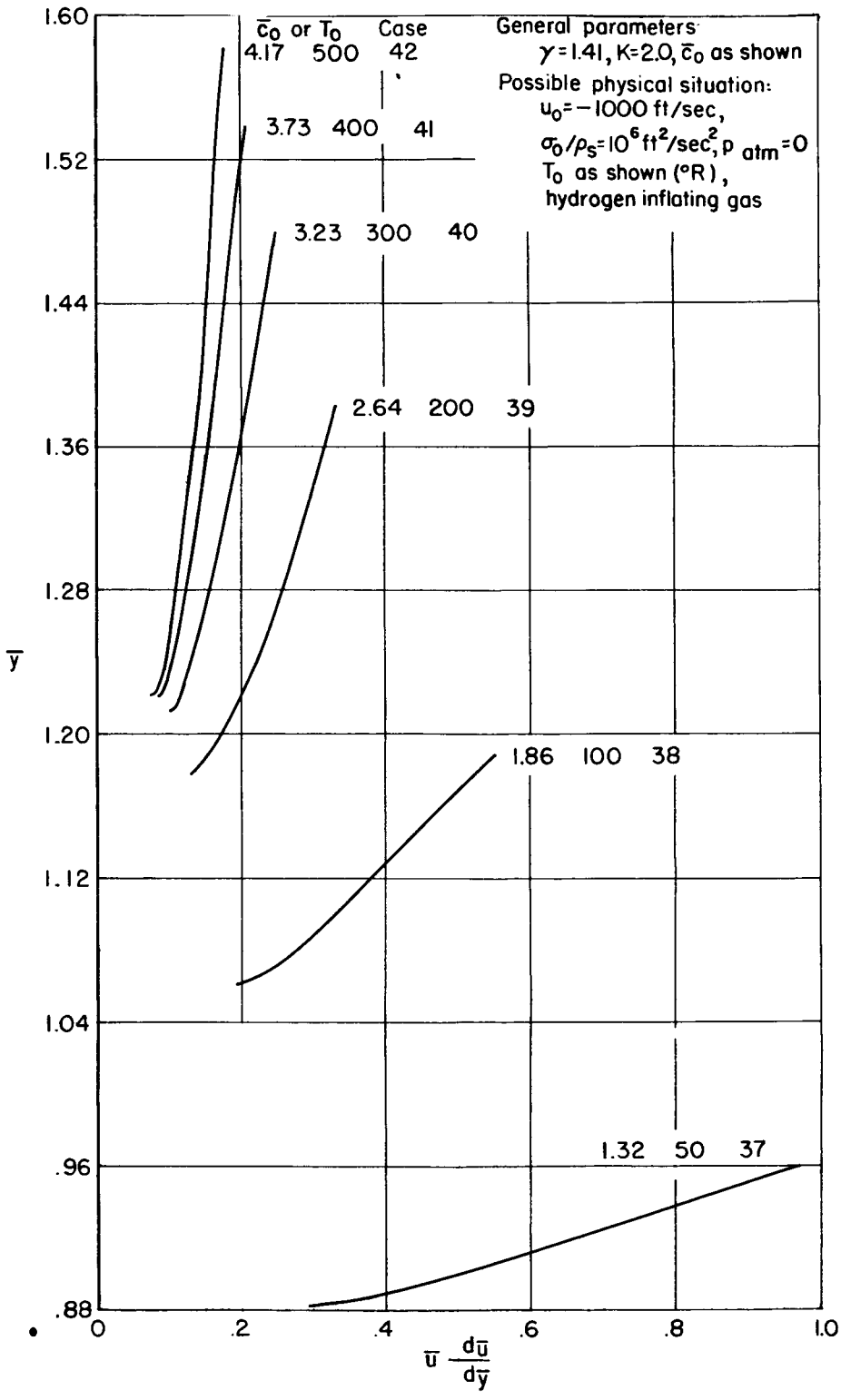

Figure 8.- Acceleration of top of sphere; K = 2.0.

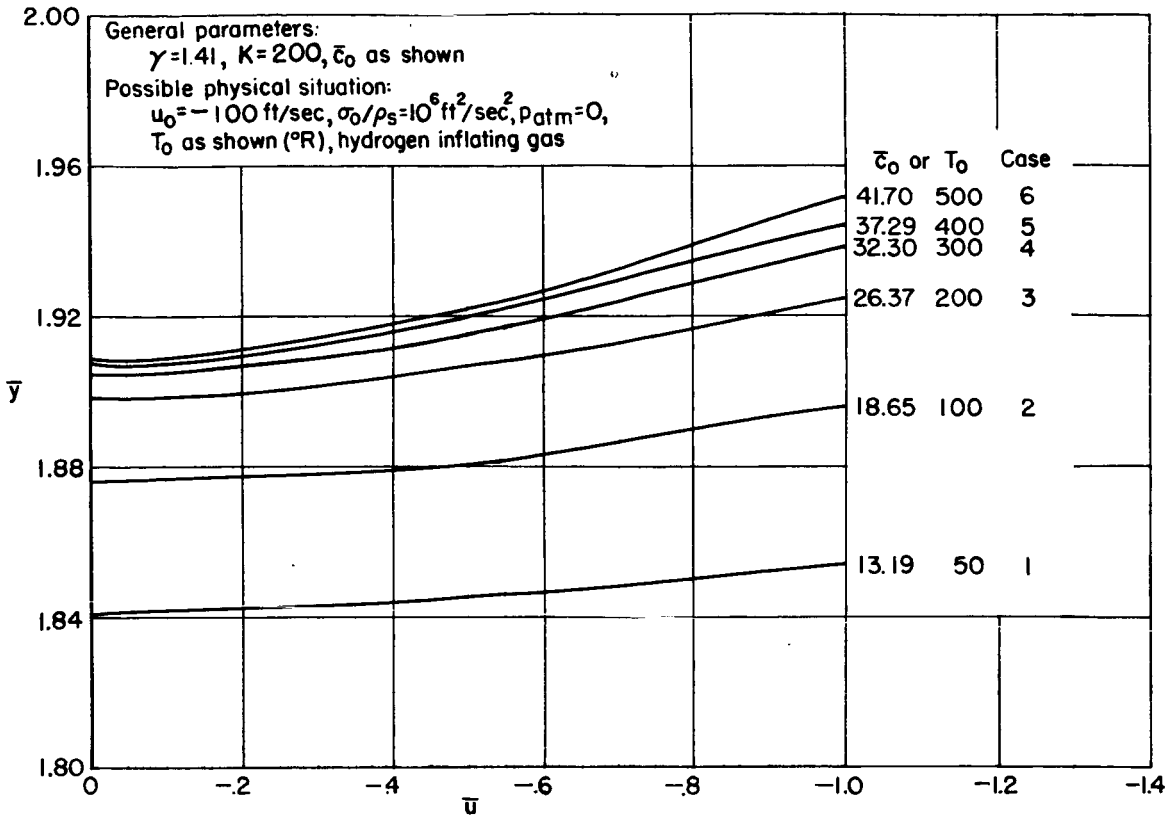

Figure 9.- Velocity of top of sphere; K = 200.

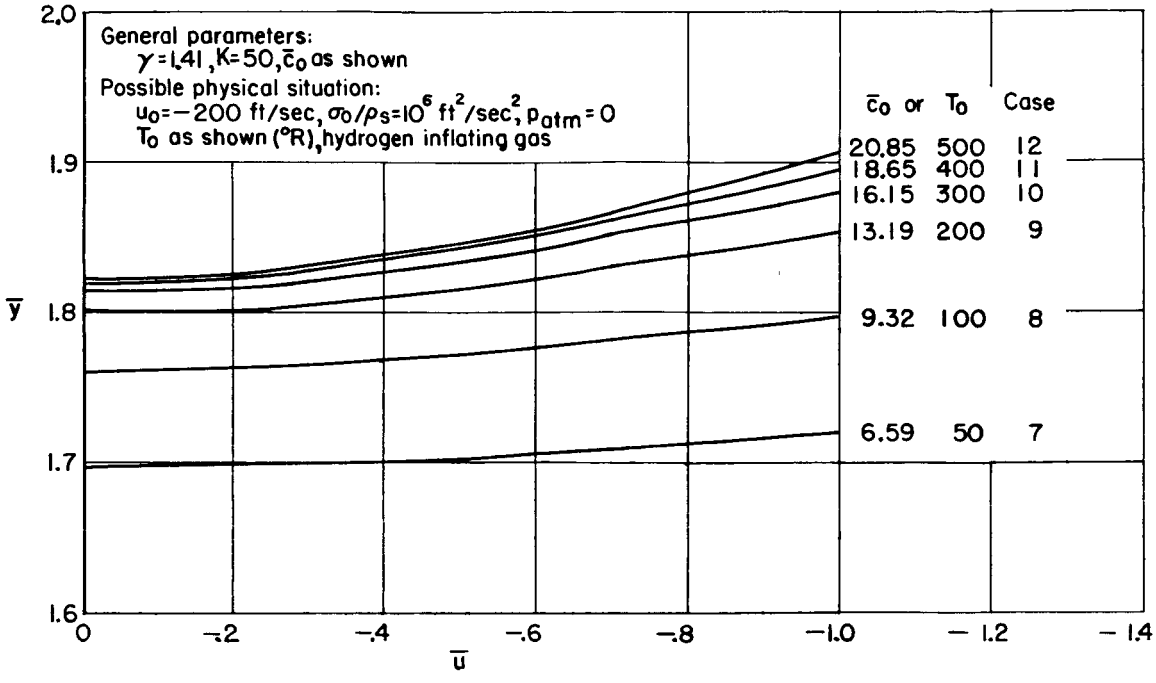

Figure 10.- Velocity of top of sphere; K = 50.

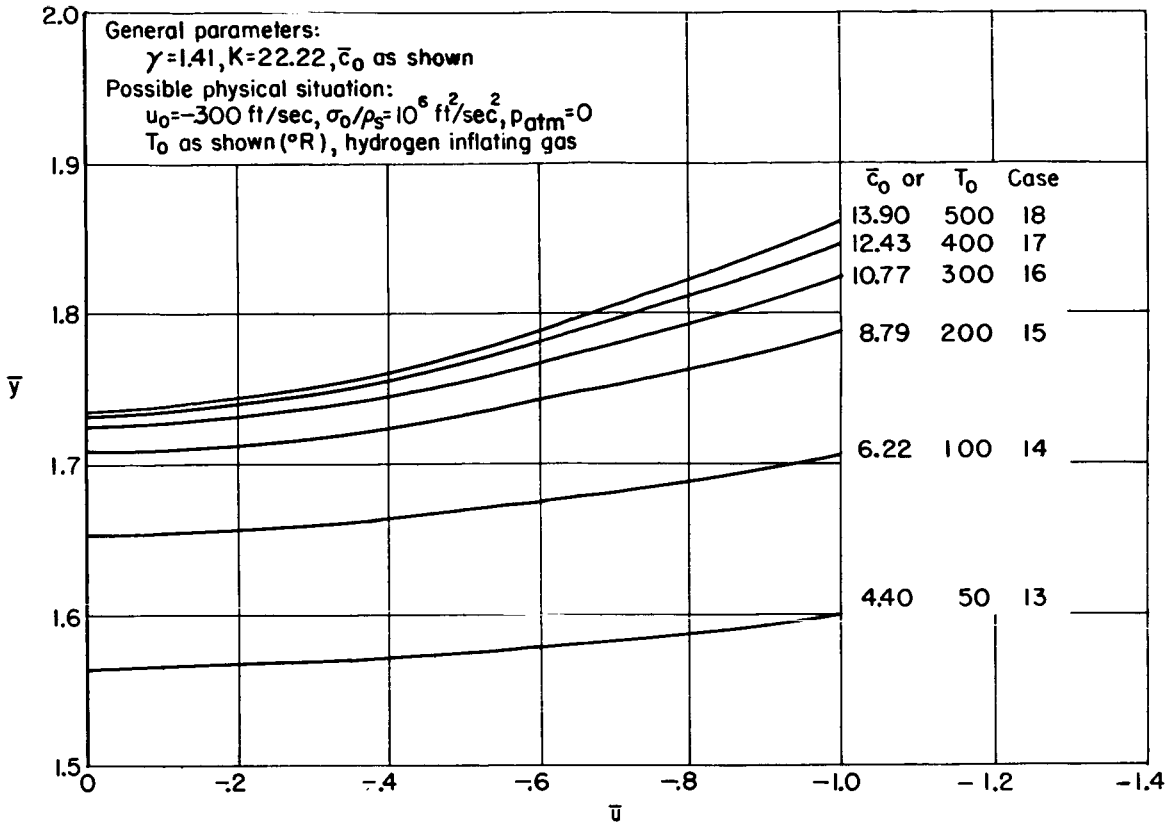

Figure 11.- Velocity of top of sphere; K = 22.22.

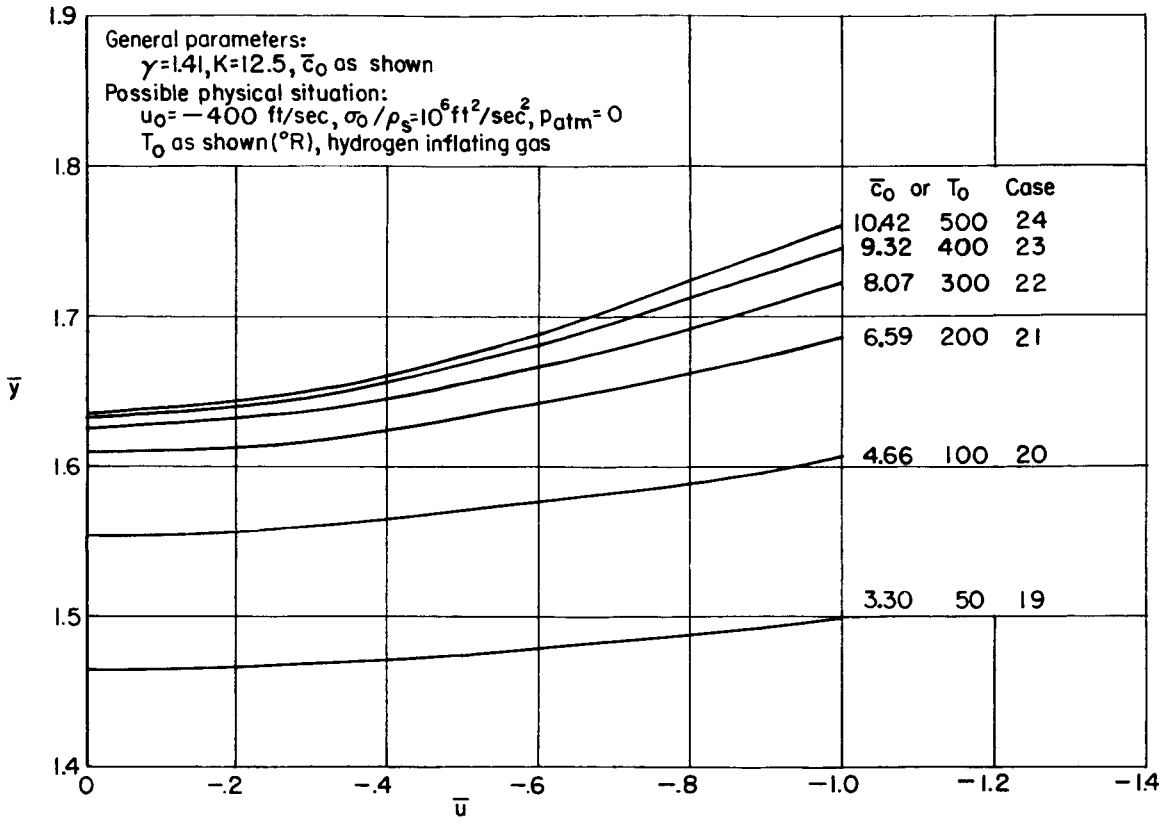

Figure 12.- Velocity of top of sphere; K = 12.5.

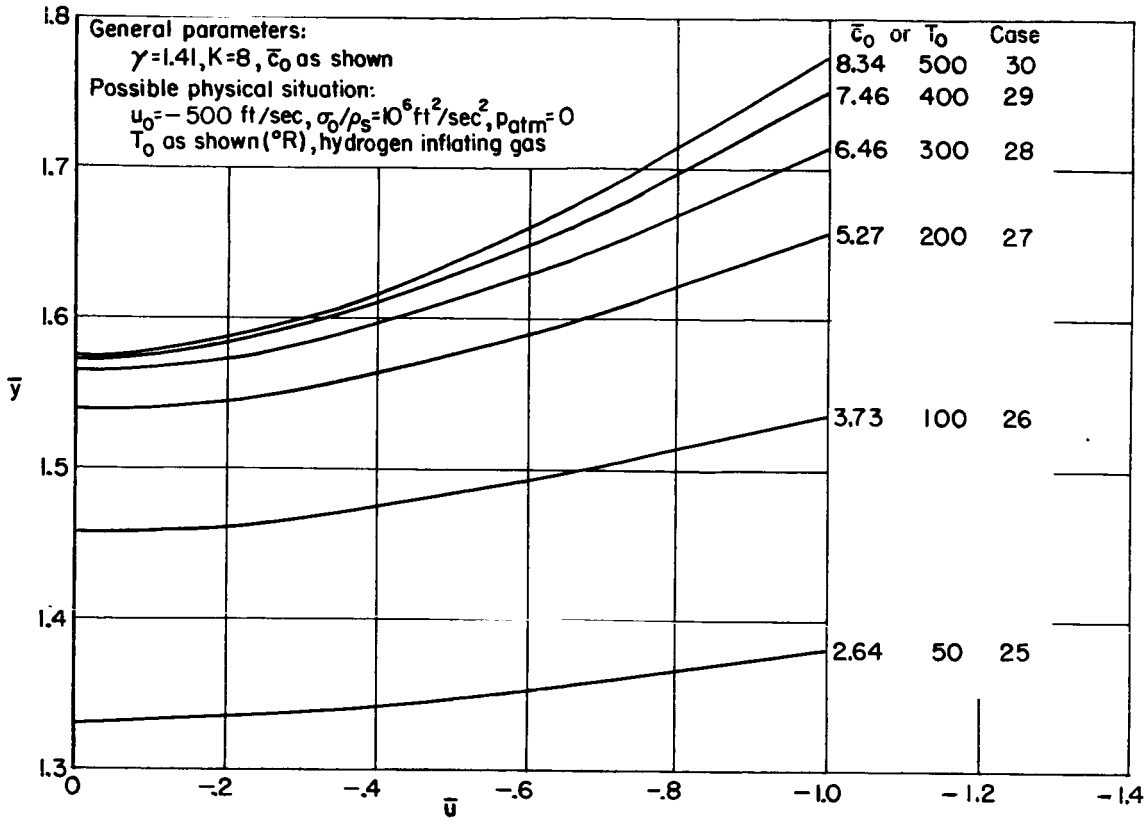

Figure 13.- Velocity of top of sphere; K = 8.

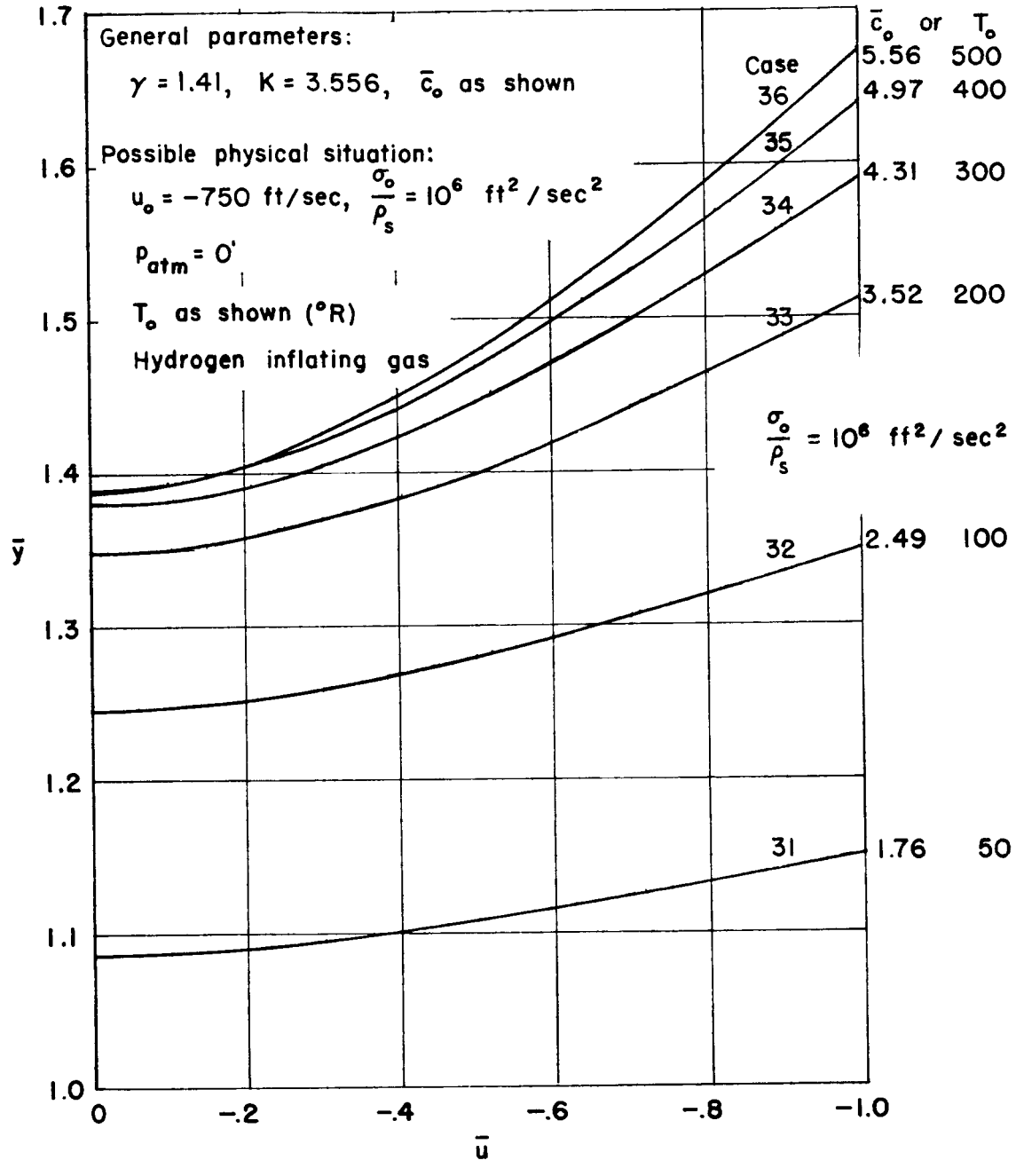

Figure 14.- Velocity of top of sphere; K = 3.556.

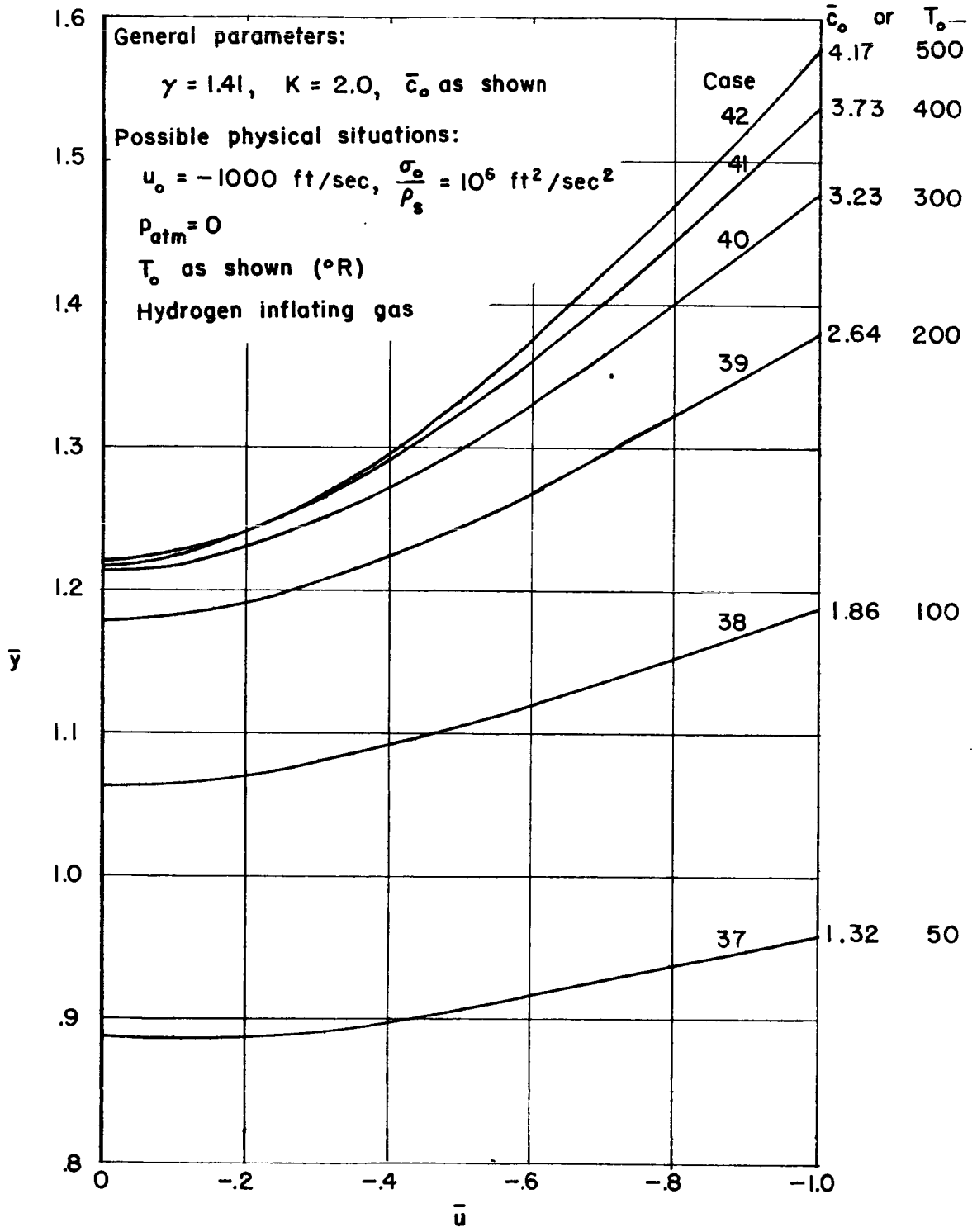

Figure 15.- Velocity of top of sphere; K = 2.0.

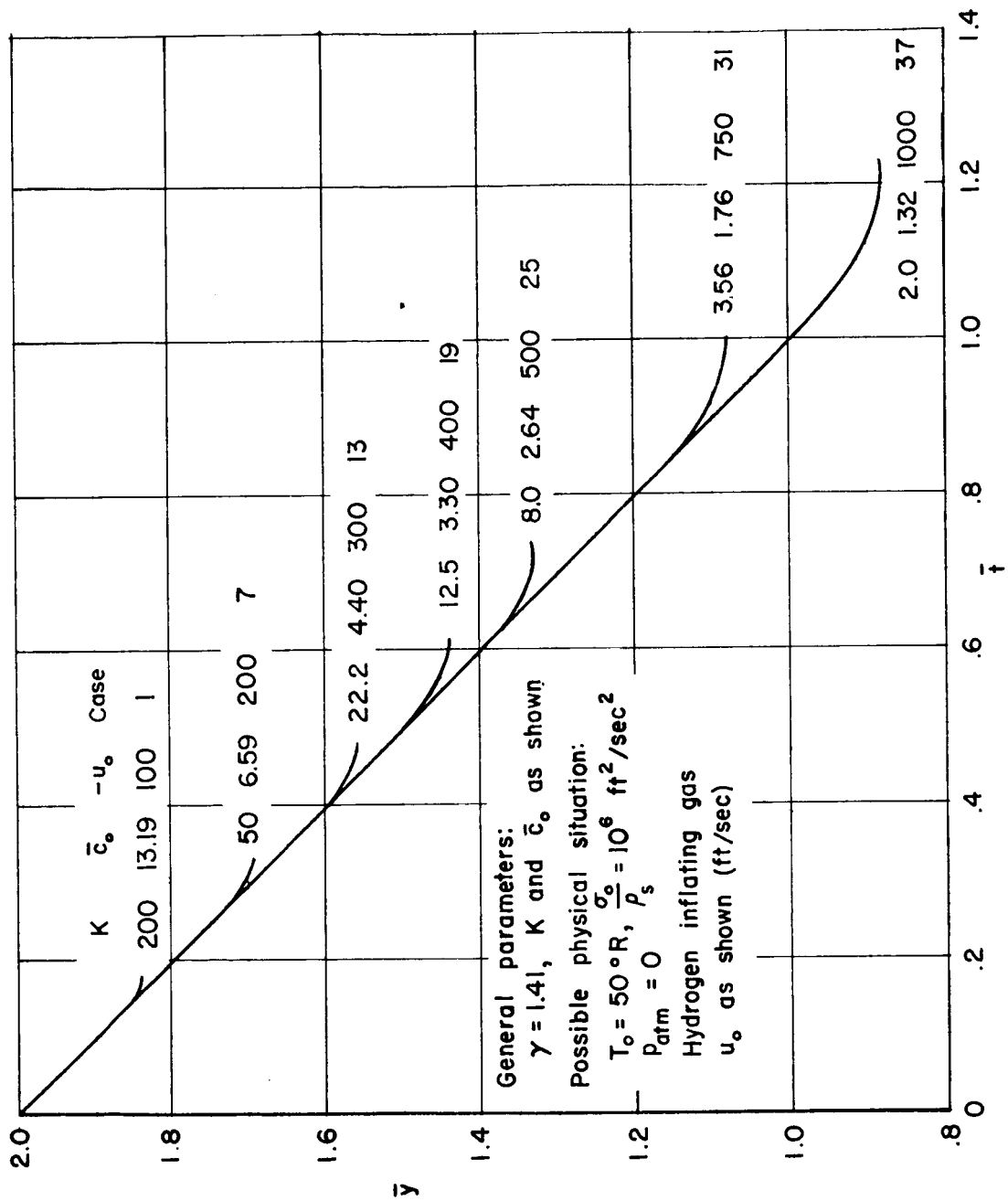

Figure 16.- Path of top of sphere; $T_o = 50^o$ R.

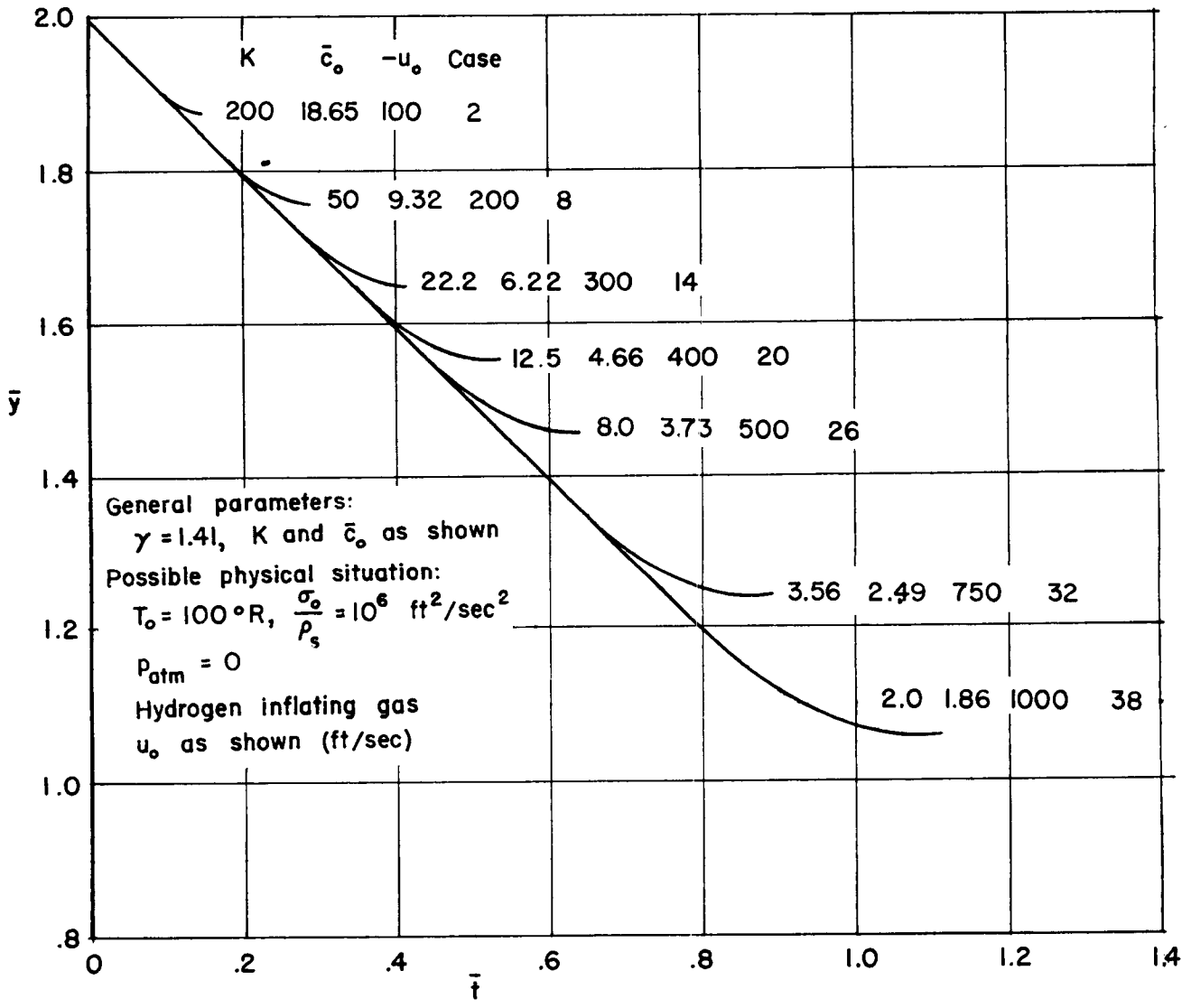

Figure 17.- Path of top of sphere; $T_o = 100°$ R.

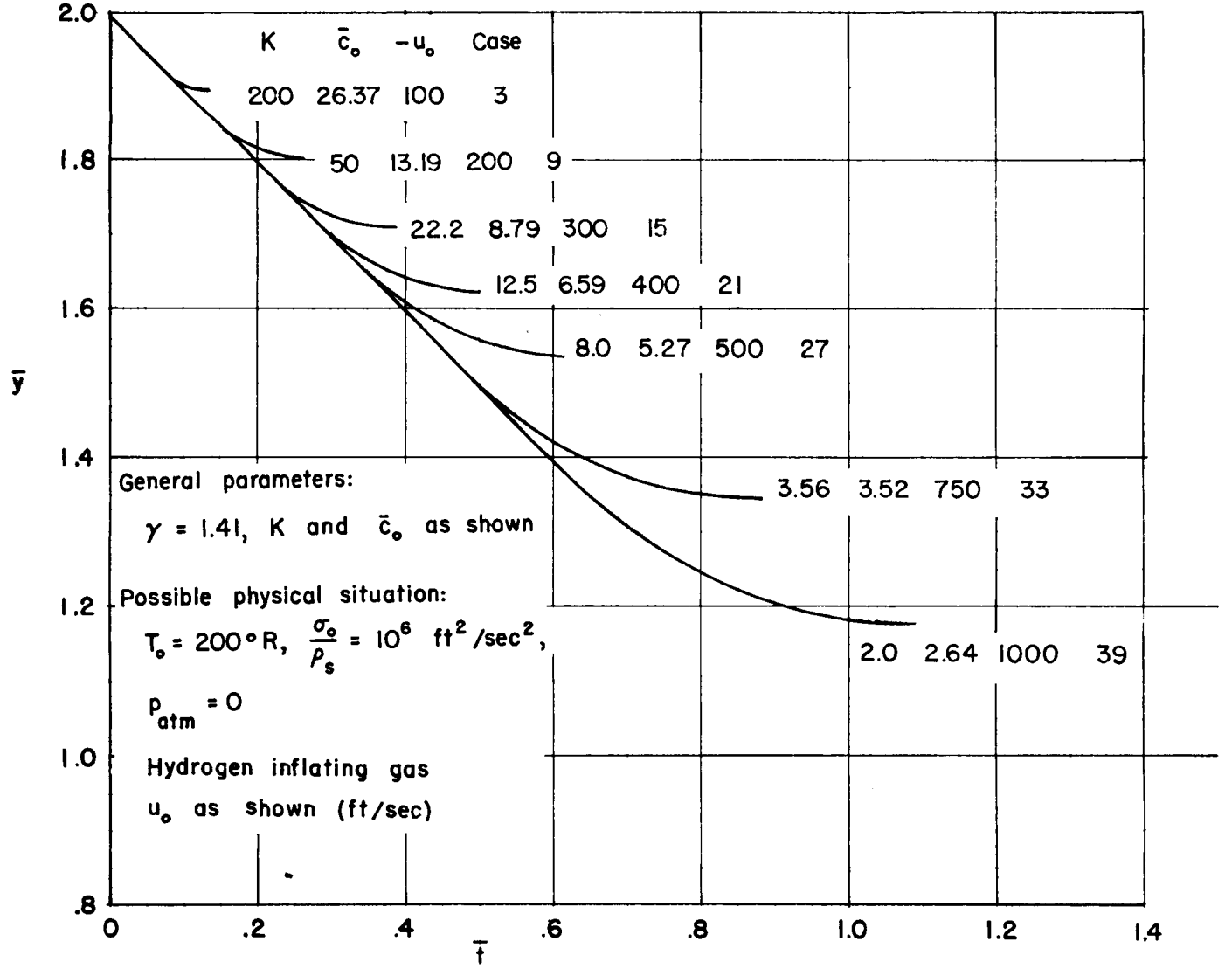

Figure 18.- Path of top of sphere; T_o = 200° R.

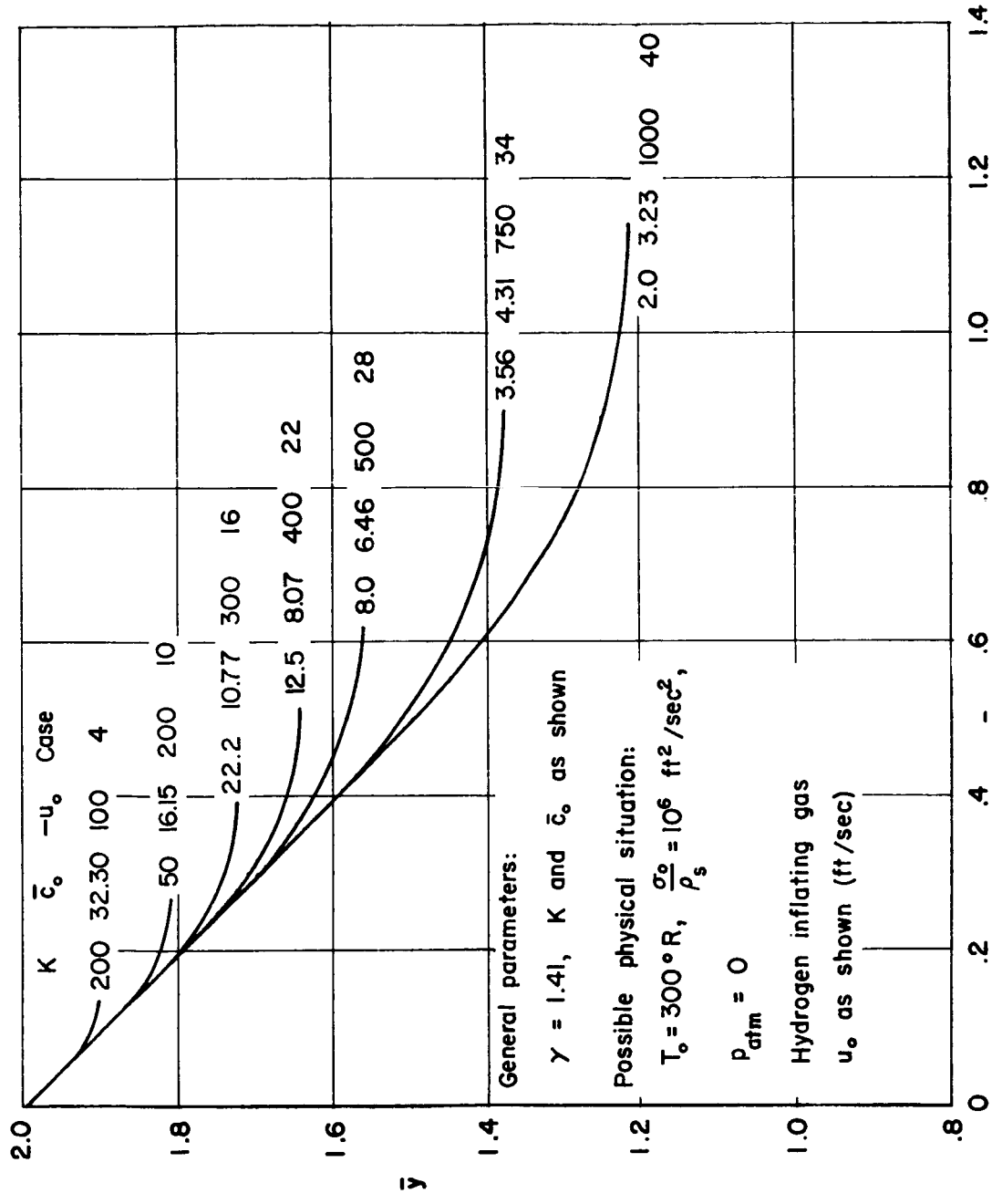

Figure 19.- Path of top of sphere; $T_o = 300^o$ R.

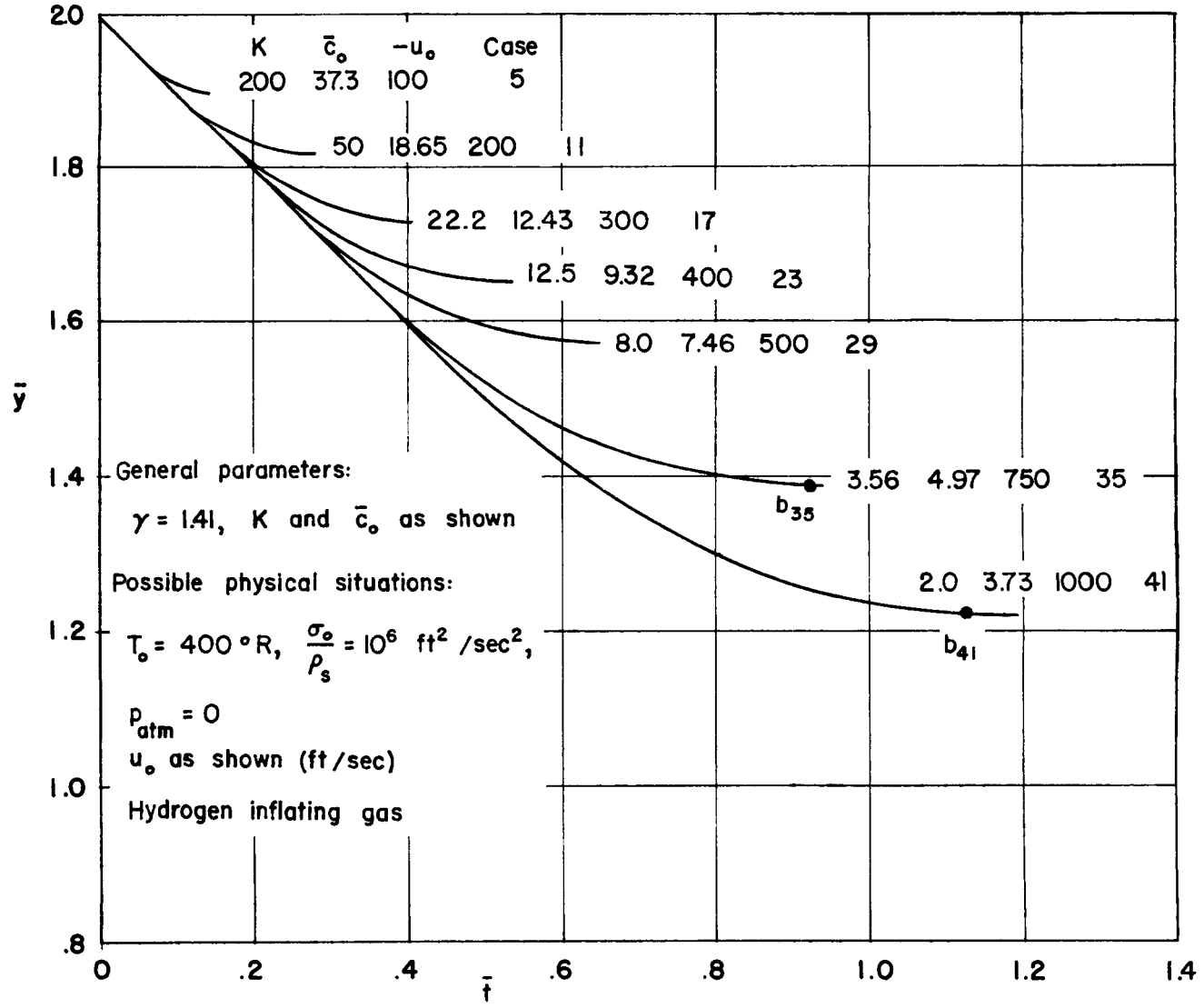

Figure 20.- Path of top of sphere; $T_o = 400°$ R.

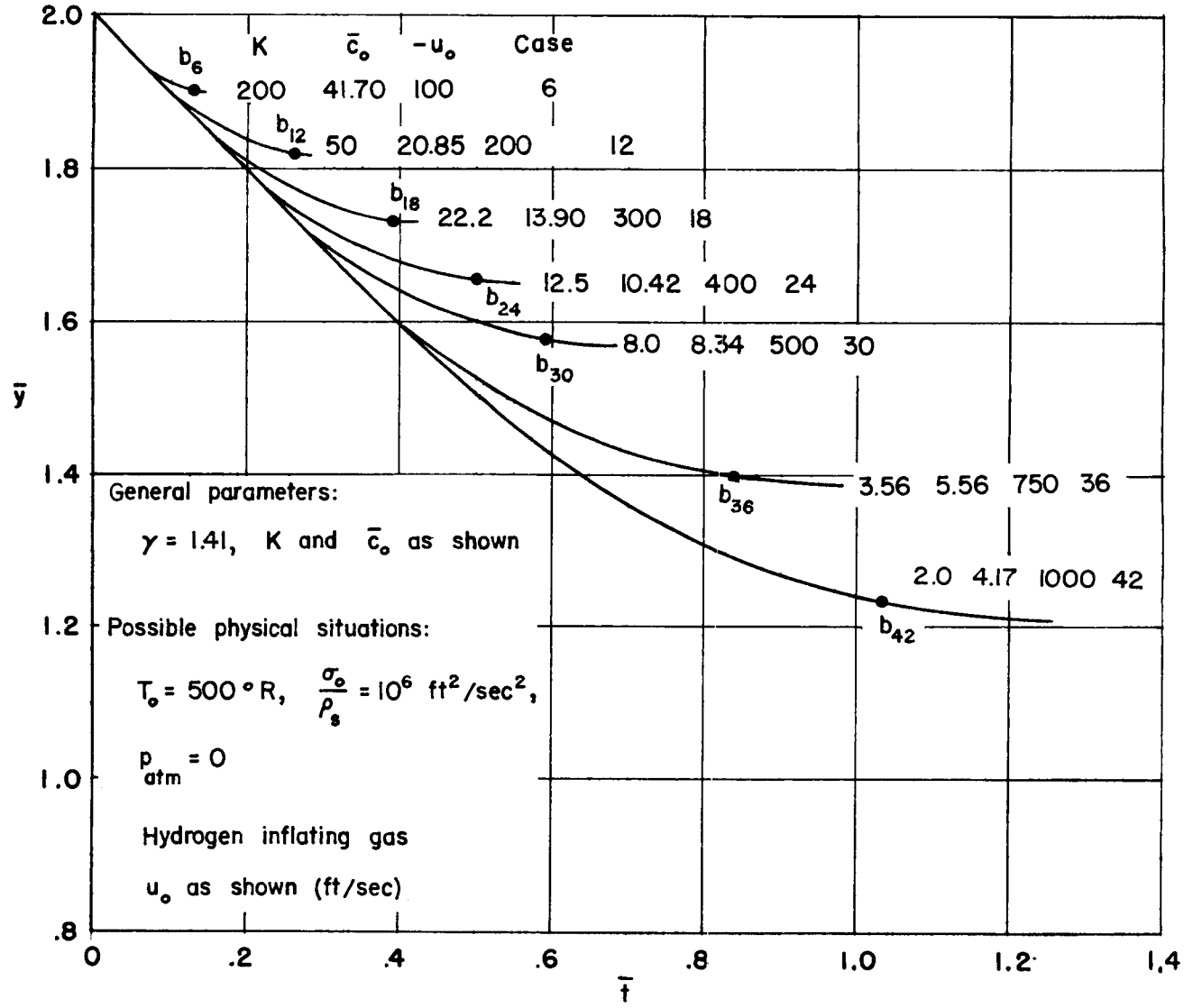

Figure 21.- Path of top of sphere; T_o = 500° R.

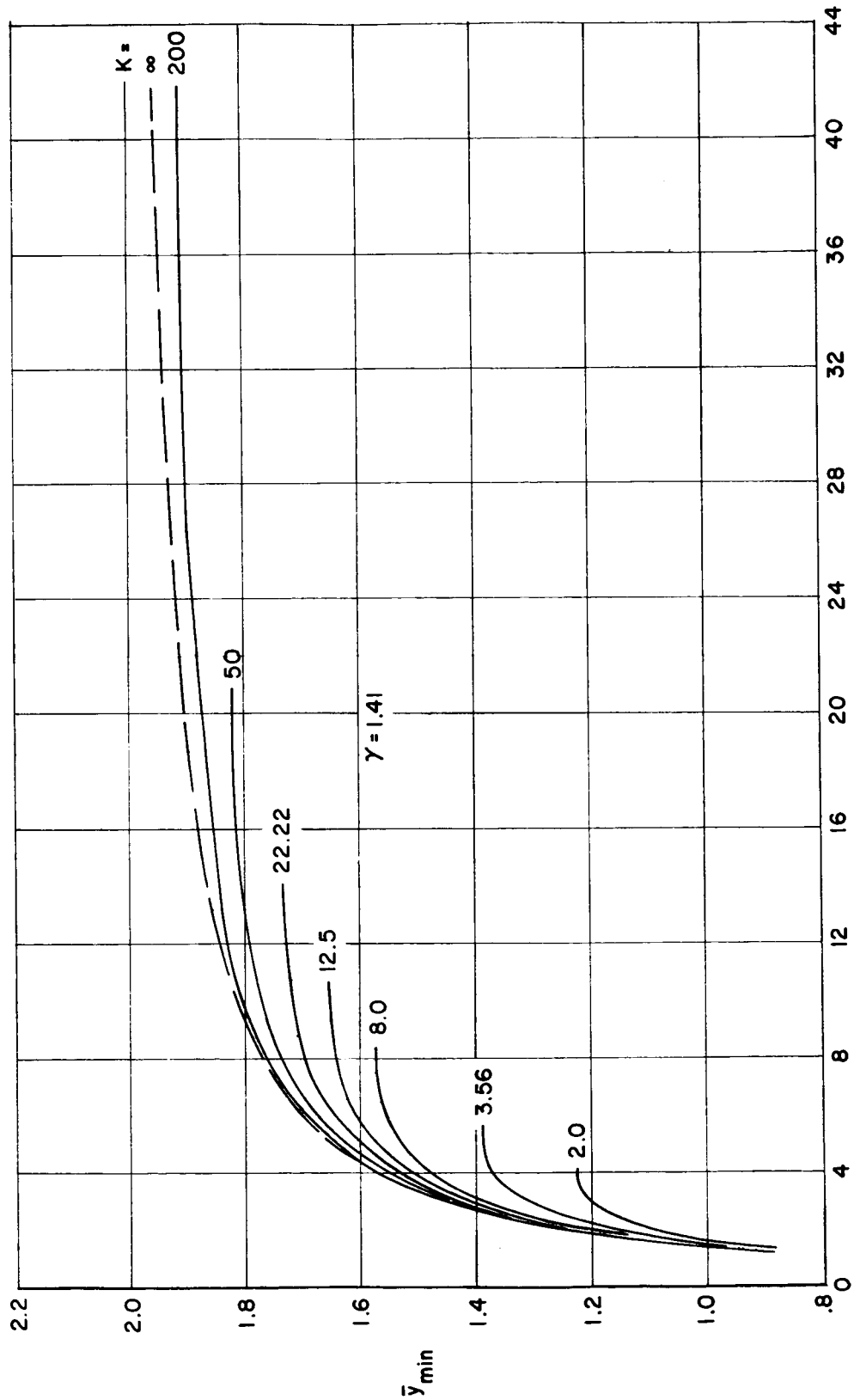

Figure 22.- Maximum deformation.

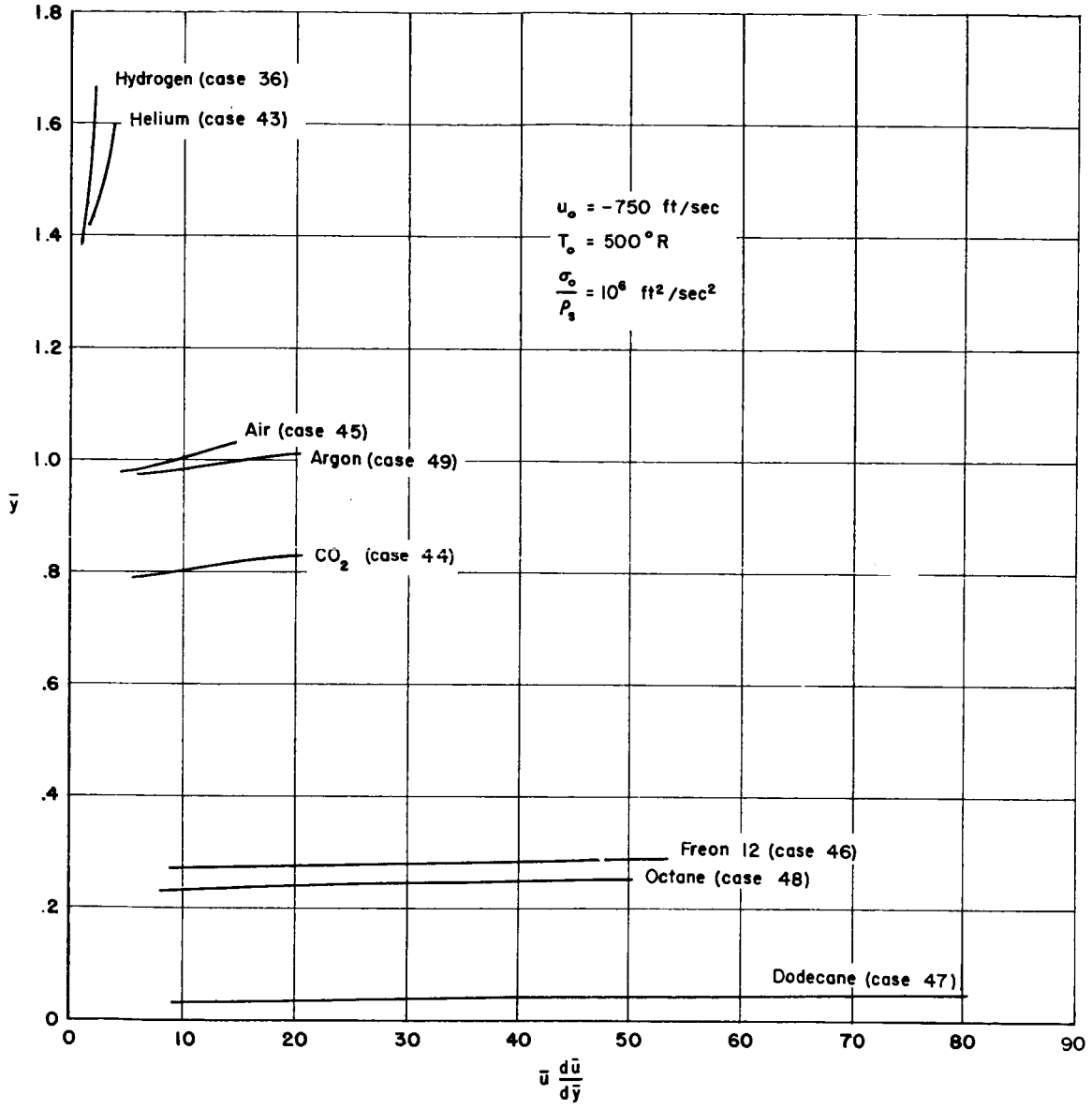

Figure 23.- Effects of various gases on acceleration.

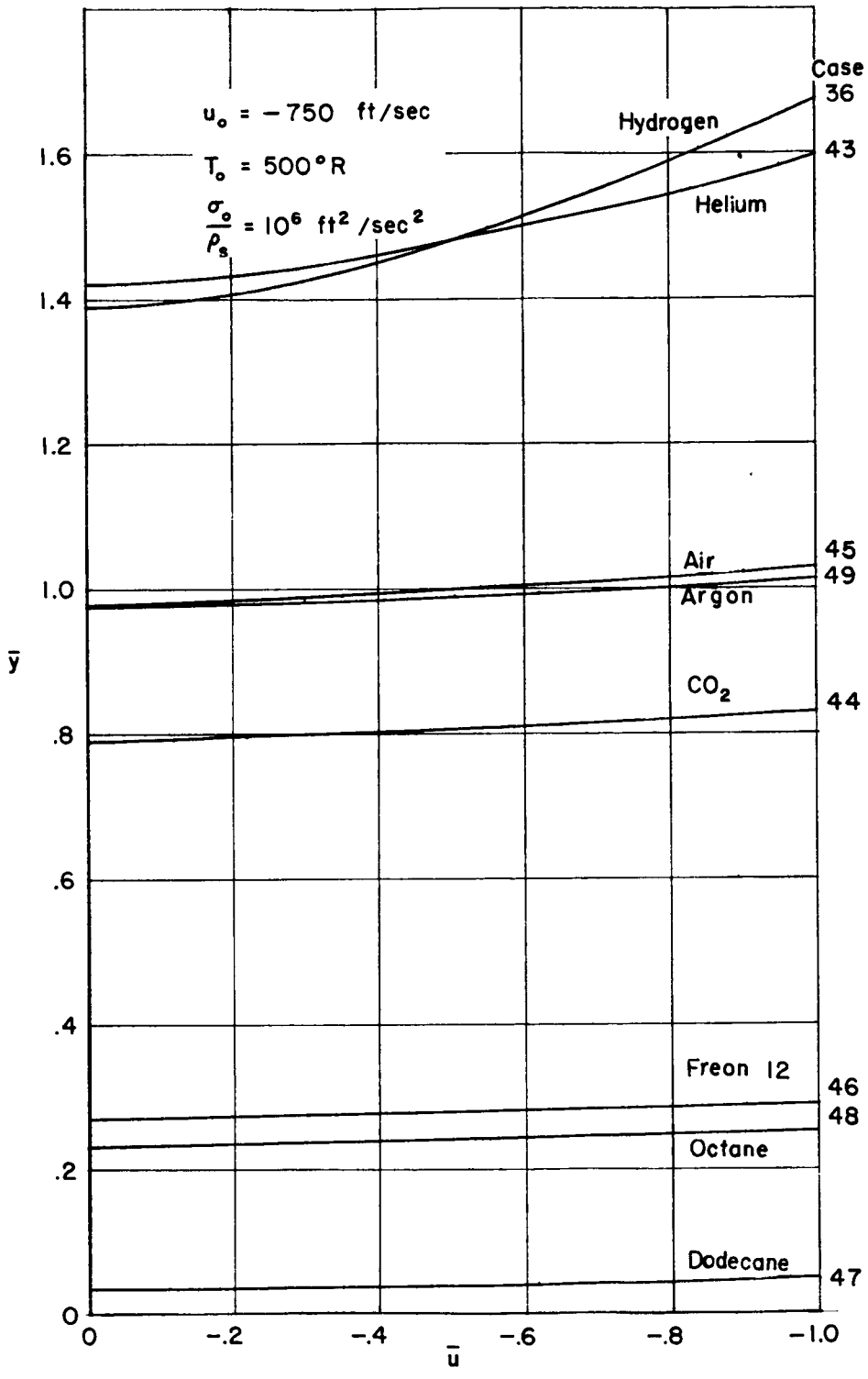

Figure 24.- Effects of various gases on velocity.

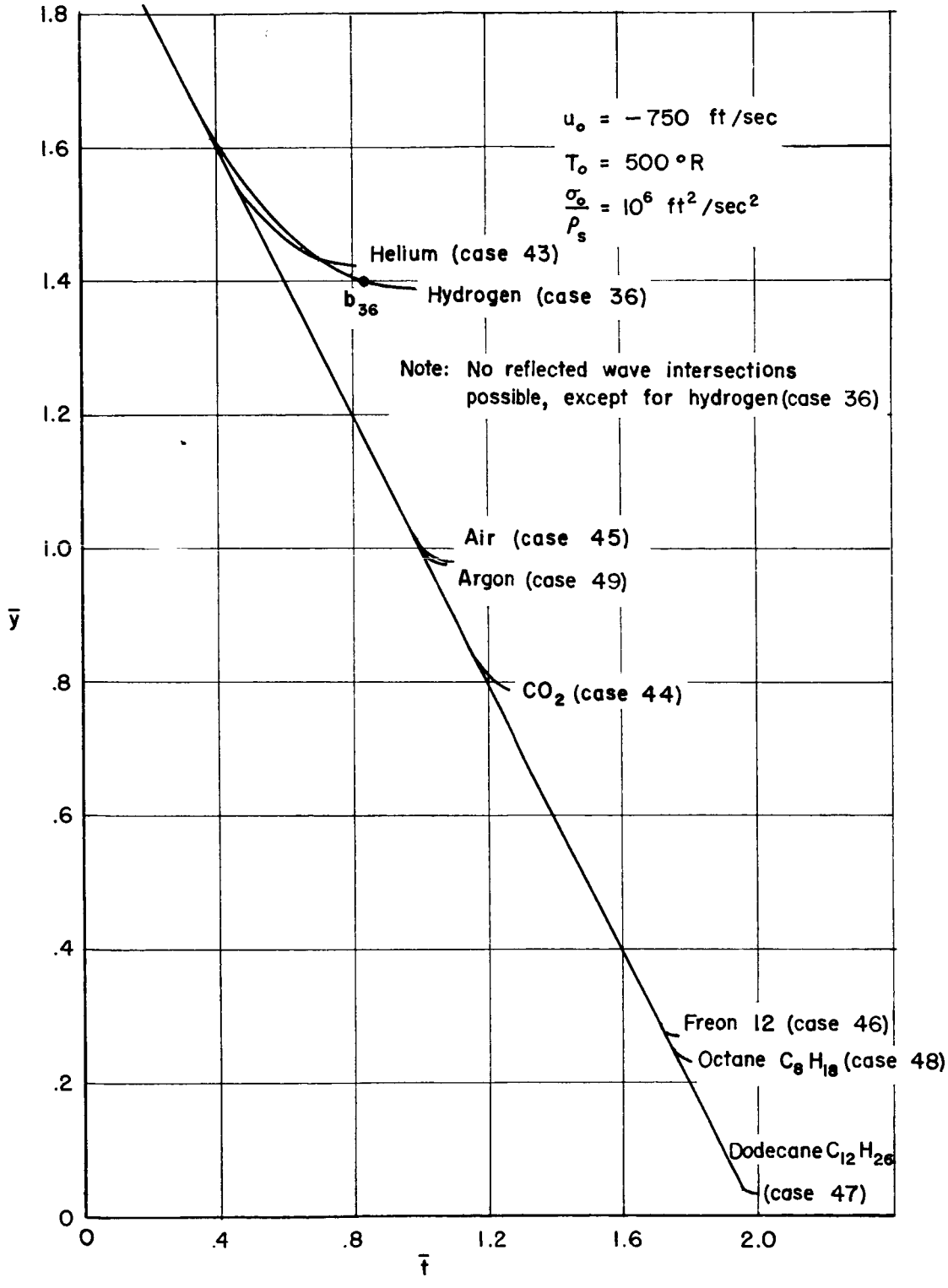

Figure 25.- Effects of various gases on trajectory.